Communication Link Model using Trellis Coded Modulation for 5G Communication in The Tropical Regions

Trilochan Patra (trilochanpatra266@gmail.com)
Techno International New Town
Swarup Kumar Mitra
MCKV Institute of Engineering

Research

Keywords: MIMO Systems, BER performance, Trellis coded modulation

Posted Date: November 18th, 2020

DOI: https://doi.org/10.21203/rs.3.rs-110209/v1

Communication Link Model using Trellis Coded Modulation for 5G Communication in the Tropical Regions

Trilochan Patra[1*], Swarup Kumar Mitra[2]
[1]*Techno International Newtown, Rajarhat, Kolkata, West Bengal, India*
[2]*MCKV Institute of Engineering, Liluah, Howrah, West Bengal, India*
[*]*e-mail: trilochanpatra266@gmail.com*

Abstract

Signal fading is a major problem in the tropical regions. Here the signals get highly attenuated for torrential rain, hence the signal power diminishes and the bit error rate (BER) increases. To enhance the signal to noise ratio (SNR) or to minimize the BER a communication link model using trellis coded modulation (TCM) for 5G communication has been proposed in this paper for the tropical regions. Various diversity techniques have been applied to minimize BER in the tropical regions. STBC (Space-Time Block Coding) MIMO technique is a spatial diversity technique which has been used in the proposed model in this paper. Bit error rate values are obtained for MIMO multipath fading distributions viz. Rayleigh fading distribution and Rician fading distribution. BER values are also attained in respect of different MIMO techniques (2x2, 3x3 and 4x4). The 4x4 STBC MIMO System has been generated using hardware co-simulation block and the results are implemented in Xilinx kintex-7 FPGA board. From the analysis of the result it is observed that Rayleigh fading distribution reflects better performance than that of Rician fading distribution. 4x4 MIMO Technique renders better result in comparison with that of lower MIMO techniques.

Keyword: MIMO Systems, BER performance, Trellis coded modulation

1. Introduction

Recently the researchers and the developers have embarked on a major revolution in establishing 5G communication on the top-of-the wireless communication to enrich the modern technology of modern civilization. Rainfall detection is also one of the major problems facing the propagation of mm waves in 5G waves [1]. Mm-wave signals are drawn, transmitted, reduced, and interrupted by rain. This practice prevents the propagation resulting in high signal loss because of the length of the propagation path [2] [3]. Rainfall rate increases dramatically as the operating frequency, rainfall frequency, or effective height increases. This phenomenon reduces the reliability, availability, and performance of the communication link. Thus, the spectrum becomes useless in cellular communication of 5G system. To create the above scenario in the negative phase, radio links in that range use multiple input and multiple output (MIMO) methods. Multiple–input multiple-output (MIMO) referred to as the use of multiple antennas at the transmitter as well as the receiver section has been originated as a key technology for 5G communication to enhance the capacity of system. Network of 5G communication uses mm Wave frequencies to supply high data transmission rate[4].Transmission and receipt of various pulses have been taken into account to activate multiple transmission channels [5] [6]. MIMO techniques transmit as well as receive multiple data signals from a standard channel. The infrared multipath exhausted area is effectively used in multiple input and multiple output (MIMO) systems to dramatically enhance the system capacity [7]. The channel capacity of MIMO system relies on the number of transmitting (TX) and receiving (RX) antennas, SNR (signal-to-noise ratio), the state of the channel and the auto correlation matrix of the transferred signal point.

The proposal has been made on the basis of the diagnosis of the MIMO channel and the capacity analysis of the aforesaid channel for 5G communication system in [8] [9]. The principal objective of [10] is to enquire about the modern wireless user (UE) hardware technology and also to identify critical issues for 5G UE hardware in circuits. In addition to this work a new design of 5G mobile user equipment, i.e. distributing incremental arrays depending on MIMO (DPA-MIMO) has been proposed. The major object of [11] is to outline the channel assessment process to reduce the drawbacks related to extra overhead added to the transmitted signal. The aforesaid process depends on the composition of contractive sample matching and scarcity flexible matching tracking method. It also transpires from [11] that the signal sources in MIMO system are gradually distributed according to local integration. This distribution method enables the use of sample compression methods to solve the drawback of channel evaluation in MIMO systems. From the findings of previous research work of 5G communication, it is observed that no such type of work using trellis coded modulation has been implemented for the tropical regions. The efficacy of the work in this paper relates to the design of communication link model for 5G Communication using MIMO technique in the tropical regions. Trellis coded modulation (TCM) has been used in this proposed communication link model. Trellis coded modulation is an effective method to reduce power requirements without increasing bandwidth [12] and this modulation also enhance the accuracy of a digital transmission system without reducing data rate.

In this paper, section 1 depicts the introduction part. Section 2 describes the methodology part. Section 3 depicts rain attenuation in tropical regions. Section 4 describes the trellis coded modulation. Sec 5 illustrates 4x4 STBC MIMO System. Sec 6 displays the proposed model. Sec 7 exhibits the result analysis part. Sec 8 indicates the conclusion part and in fine, references are described.

2. Methodology

A communication link model using trellis coded modulation for 5G communication has been devised for the tropical regions in this paper. As the signal gets highly attenuated because of heavy rainfall, the diversity technique i.e. 4x4 MIMO technique has also been used in this communication link model. The details of proposed communication link model and hardware design of 4x4 STBC MIMO has been described in section 6 of this paper. The result analysis has been classified into two categories-simulation part and hardware implementation part. The simulation part has been worked out using MATLAB. The hardware part has been computed using system generator and implemented by applying Xilinx Kintex-7 FPGA kit. An algorithmic approach depicts high level synthesis of the proposed communication link model step by step and this has been demonstrated below in figure 1-

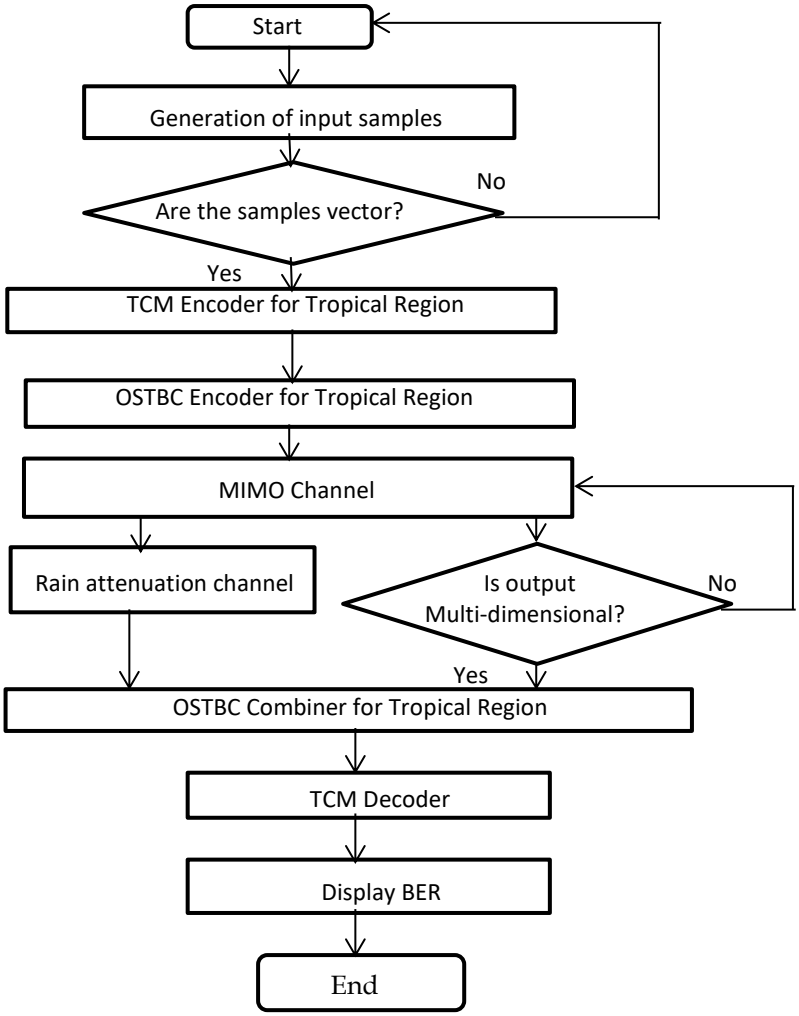

Fig 1: Flowchart of the proposed communication kink model

.

3. Rain attenuation in tropical regions

Total precipitation [13] [14] has been calculated on the basis of the amount of attenuation that arises out of rainfall per unit area. The amount of attenuation per unit volume is defined as the Specific Rain Attenuation measured at [dB / km]. Calculation of specific rainfall is detected especially in relation to the degree of rainfall with symptoms like storms and electric waves at that particular place. The characteristics of rain embrace precipitation and raindrop size whereas the characteristics of the electromagnetic waves comprise the frequency band, the polarization type and the propagation index. The acquisition of a particular rainfall is further propagated by the propagating electromagnetic waves. Its impact changes relying on temperature of water, ratio of water and frequency belts of operation. Thus, the electromagnetic wave is absorbed by the rain and gets dissipated as heat and the remaining portion of the electromagnetic wave which is not absorbed is scattered in all the directions [15] as displayed in Fig.2.This scattered electromagnetic wave emits invalid signals or interferes with the input of the received signal and as a result of this, extra attenuation originates. If the wave propagation is short and comes close to the size of the raindrop, the absorption of the wave becomes higher and the propagation becomes greater. As a result, the absorption and propagation of the electromagnetic wave depend on the operating frequency, the rainfall rate, the composition of the rainfall and the size of the raindrop. Therefore, the estimation of precipitation depends on the rainfall rate and frequency regression coefficients. Here, the specific rain attenuation is considered as γ and represented numerically in Equation 1 given below:-

$$\gamma = KR^{\propto} \qquad (1)$$

In equation (1) stated above R denotes rain rate and both k and $\propto$ denote power law parameters which rely on different factors like distribution of raindrop size, temperature, frequency of operation and emission of electromagnetic radiation. The specified attenuation of rainfall is based on the category of polarization of electromagnetic waves because of round shape nature of raindrops. The attenuation rate which arises from the vertical polarization waves is smaller than that which is caused by horizontal polarization [16] [17]. The values of parameters k and $\propto$ have been reflected in ITU Rec. P.838-3 [18]. The available rainfall area shown in Equation 1 above illustrates the distribution of rainfall ranging one kilometer while the length of the total rainfall area between the transmitter and the receiver is calculated by the frequency of the particular rainfall γ and by the actual length of the path L_{ac} if it is observed that rainfall has been scattered uniformly. If the rainfall is not uniformly scattered along the length of the wireless path, the calculation of rain attenuation based on the length of the actual path produces undesired results. In view of what is stated above, the horizontal uniformity of precipitation has been chosen. This incident has been identified as the effective length of path of the connection between the transmitter and the receiver and this effective length of path must be less than the actual wireless path length. This above phenomenon has been applied to assess the actual path length between a transmitter and a receiver for the uniform spreading out of rainfall. On the basis of the above phenomenon, the length of the effective path has been accepted as an important factor to analyze the rain attenuation. To compute

the effective path length L_{eff}, the minimization of the distance has been considered to measure the actual length of the path in case of a uniform spreading out of rainfall. So, a new metric has been suggested and it is defined as a distance deduction factor "d_r" used to compute the effective path length between a transmitter and a receiver. The effective path length calculated in terms of mathematics is established on the basis of the length of the sphere itself L_{ac}, between two sides of the interaction and the assumptions about the structure of the rainfall equation for the structural distribution. Therefore, the effective path length has been mathematically demonstrated in Equation 2 [18] [19] [20] below:

$$L_{eff} = d_r L_{ac} \qquad (2)$$

In the equation (2) above L_{eff} denotes the length of the effective path, d_r indicates the distance deduction factor or distance factor as recommended by ITU [21] and L_{ac} represents the actual length of the link between a transmitter and a receiver. Different kinds of significant predicted models have been designed and suggested by different researchers in different times to assess the horizontal rainfall variability in the tropical regions [22] [23]. The most popular model used in the tropical region is ITU-R model. This model has been analyzed as an outcome of frequency with rain rate 0.01% of the time, the executant in the specified attenuation model and the real path length. Although the ITU-R model has been used to find out the amount of precipitation fluctuations, it is not the appropriate model for the tropical regions. Therefore, a number of models such as updated Silva Mello model [24], Abdulrahman's model [25], and Lin's model [26] have been matured and used to assess the path deduction factor.

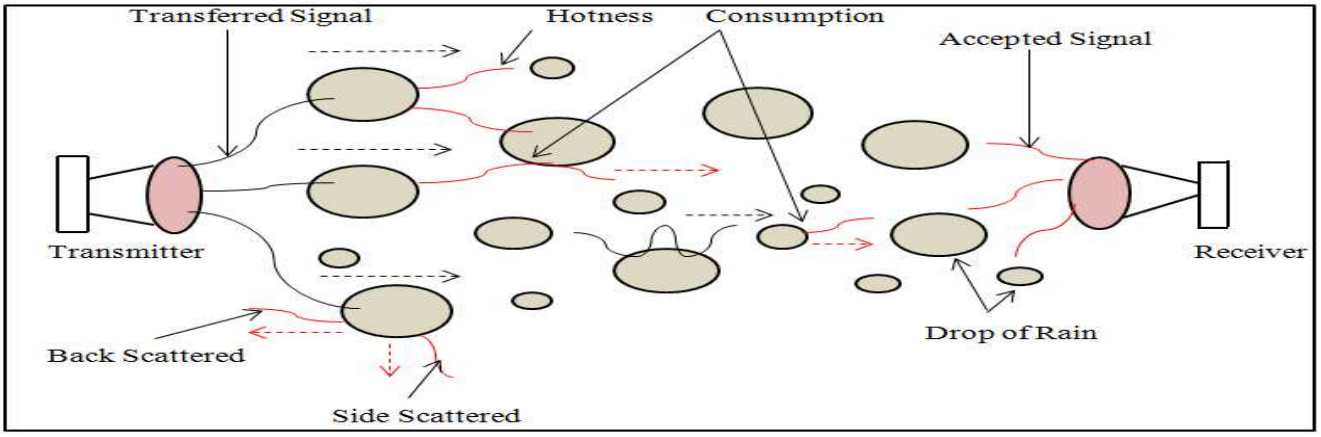

Fig.2. Rain impact on electromagnetic wave propagation

4. Trellis coded modulation

The trellis codes for band-limited channels arise out of combining convolution coding with modulation. This state of combining is itself called as trellis coded modulation (TCM). This form of signaling comprises two basic features-the first feature is that the number of signal points lying in the constellation used is greater than what is used for the modulation format of interest with the identical data rate. Here the surplus points permit excessiveness for forward error control coding without giving up bandwidth. The second feature is that convolutional coding is utilized to bring in certain reliability between successive signal points such that only certain patterns or sequence of signal points are allowed.

In communication system, the channel volume curves [27] suggest that doubling the number of generated signals improve the reliability of digital communication system over an additive white Gaussian channel by maximum 6dB. In other words, if the k_b bits are to be transmitted, then using the letters A′ of $2k_b + 1$ and utilizing the proper encoding scheme, it is likely to significantly increase the effectiveness of digital communication system against the extra noise. This is performed by providing a standard computer installer at the rate $R = K_b / (K_b + 1)$ and binary input data and then mapping the result $(K_b + 1)$ of the code words to the alphabet. This framework was originally proposed by Ungerboeck in 1982 [28]. Again the TCM functions contain the Trellis code and the constellation mapper as shown in Figure 3. TCM includes the coder functions of rate $R = K_b / K_b + 1$ and an M-Ary display showing $M = 2^{kb}$ input maps to a large constellation of $M = 2^{kb+1}$ point locations.

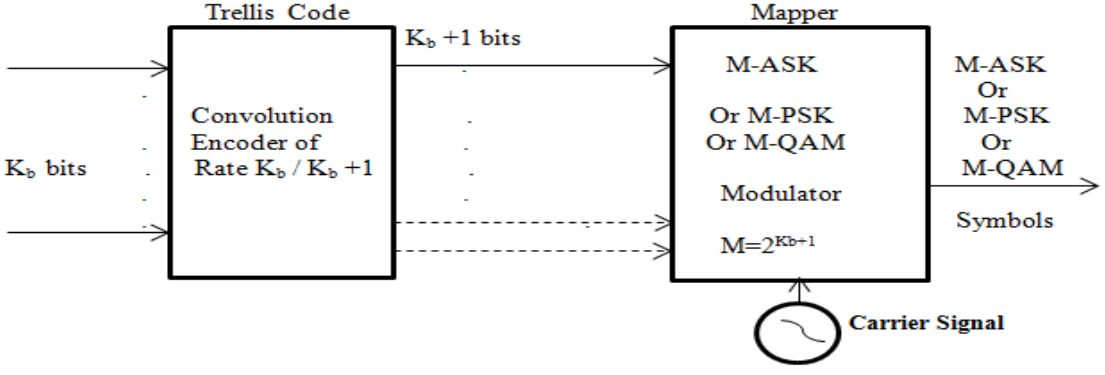

Fig.3. A simple Trellis Code Modulation

When a sequence of emitted signals $\{S_b\}$ get polluted by additive white Gaussian noise (AWGN), the decoder starts beginning to create erroneous decisions, perhaps being engaged in a trellis path that is separated by more than one transmission from the real path. Such errors are called incident-events. When Viterbi decoding is used the probability of such errors are estimated at very high signal-to-noise-

ratio (SNR) and the probability of such errors P′ is mathematically expressed in the following manner:

$$P' \cong N_{E\ free}\, Q'\,(d_{E\ free}/2\sigma') \qquad (3)$$

Where Q′denotes the Gaussian error integral. N_{Efree} denotes the average number of errors with distance $d_{E\ free}$. The free distance d_{Efree} of the trellis refers to the minimum Euclidean distance between pairs of sequences $\{S_b\}$ and $\{S_b'\}$ that the encoder generates and it is mathematically displayed below-

$$d_{Efree} = \min_{S_b \neq S_b'} [\sum_{m=1}^{M} \|S_b - S_b'\|^2]^{1/2} \qquad (4)$$

On the other hand, the effective path length is computed using equation (2) for trellis coded modulation technique.

As the trellis coded modulation is an effective and efficient bandwidth technique obtained using convolution codes, it preserves bandwidth by measuring the number of points displayed. In this way the rate of bits is enhanced but the rate of symbols remains the same. Coding conversion permits the modification of symbols to create sequential codes. In trellis coded modulation the increasing of the constellation size decreases the Euclidean distance between constellation points but the sequence of coding provides a coding gain that overmatches the disadvantage of power which moves towards the level of higher constellation. Performance is measured by the benefit of encoding over a fixed signal. The Euclidean sorting criterion is not considered as the Hamming range.

By applying trellis coded modulation with STBC MIMO system, energy efficiency throughput and spectral efficiency are obtained. Besides, by using trellis coded modulation with MIMO system normalized utility power and normalized packet delay are attained. So steps have been put in STBC MIMO system.

5. STBC MIMO System

Here a code word has been taken into account and a 4x4 MIMO system has been created with that code word [29]. This 4x4 MIMO STBC (Space time block coding) caused by 2x2 Alamouti STBC to receive diversity is developed using a building code adopted by Walsh-Hadamard to detect error and code. Here four sets of symbols and four transmitting and receiving antennas have been adopted. The same concept of transmitting signals from transmitters is applicable to the construction of the 4x4 Alamouti STBC. Thereafter the symbols are twisted sharply either by mixing at random or by changing the phase and then the symbols are again transferred. This method is repeated for the other two spaces, and later this process is repeated for all information. Now it is felt necessary to mention some advantages of MIMO. MIMO is extensively applicable to increase the capacity of channels by exercising multiple antenna configurations. In the MIMO system the data rate is improved by applying spatial multiplexing but the authenticity of the system is developed by space time coding. Space time block codes have been adopted in MIMO system for enhancing the diversity gain.

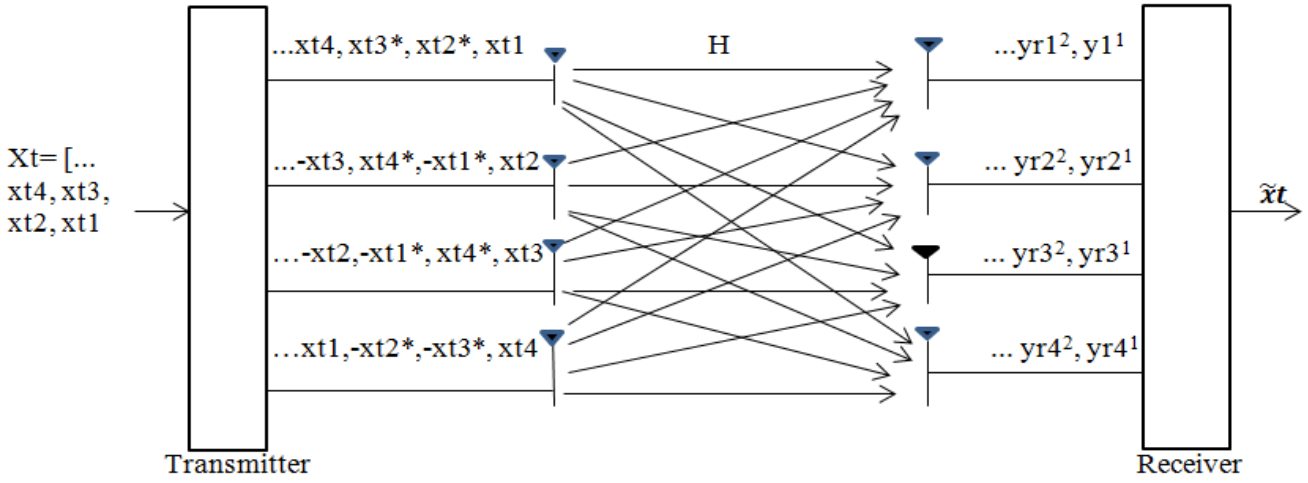

Fig.4. MIMO Channel of 4x4 STBC Systems

Let xt1, xt2, xt3, and xt4 are the symbols which are to be transmitted. In the first slot, the said four symbols are transmitted in fundamental order. In the second slot, coded symbols such as xt2 *, -xt1 *, xt4 * and -xt3 * are transferred consequently. Similarly, xt3 *, xt4 *, -xt1 * & -xt2 * and xt4, -xt3, -xt2 & xt1 are transmitted in the third and fourth time Slots. The negative signs and conjugates are used here to suggest a phase shift for supporting orthogonality which is the main property of QOSTBC (Quasi orthogonal space time block code). In the same way, the information is transmitted from four transmitting antennas in four time intervals. Now it is necessary to create 4x4 STBC transmission matrix using Walsh-Hadamard repetitive composition rule on 2x2 matrix of Alamouti transmission. The steps below describe the style of transference of coded symbols to obtain diversity.

Step 1: Considering 2x2 Alamouti transmission matrix,

$$\boldsymbol{X}t' = \begin{bmatrix} xt1 & -xt2* \\ xt2 & xt1* \end{bmatrix}$$

Step 2: considering another moving matrix set of $xt3$ *and* $xt4$ symbols,

$$\boldsymbol{X}t'' = \begin{bmatrix} xt3 & -xt4* \\ xt4 & xt3* \end{bmatrix}$$

Step 3: Replacing scalars with matrixes in 2x2 Alamouti transmission matrixes and they are denoted $\boldsymbol{X}t'$ *and* $\boldsymbol{X}t''$,

$$\begin{bmatrix} Xt' & -Xt''* \\ Xt'' & Xt'* \end{bmatrix}$$

Step 4: Putting scalar matrix values using the Hadamard matrix form to obtain a 4x4 transmission matrix as a 2x2 Alamouti type,

$$\begin{bmatrix} Xt' & -Xt''* \\ Xt'' & Xt'* \end{bmatrix} \rightarrow \begin{bmatrix} \begin{bmatrix} xt1 & -xt2* \\ xt2 & xt1* \end{bmatrix} & -\begin{bmatrix} xt3 & -xt4* \\ xt4 & xt3* \end{bmatrix} \\ \begin{bmatrix} xt3 & -xt4* \\ xt4 & xt3* \end{bmatrix} & \begin{bmatrix} xt1 & -xt2* \\ xt2 & xt1* \end{bmatrix} \end{bmatrix}$$

$$\rightarrow \begin{bmatrix} xt1 & -xt2* & -xt3* & xt4 \\ xt2 & xt1* & -xt4* & -xt3 \\ xt3 & -xt4* & xt1* & -xt2 \\ xt4 & xt3* & xt2* & xt1 \end{bmatrix}$$

Step 5*:* Changing signs for 2nd and 3rd columns, to achieve Quasi-Orthogonality,

$$\begin{bmatrix} xt1 & -xt2* & -xt3* & xt4 \\ xt2 & xt1* & -xt4* & -xt3 \\ xt3 & -xt4* & xt1* & -xt2 \\ xt4 & xt3* & xt2* & xt1 \end{bmatrix} \rightarrow \begin{bmatrix} xt1 & xt2* & xt3* & xt4 \\ xt2 & -xt1* & xt4* & -xt3 \\ xt3 & xt4* & -xt1* & -xt2 \\ xt4 & -xt3* & -xt2* & xt1 \end{bmatrix}$$

Finally, the transmission matrix is,

$$\boldsymbol{X}\text{t}=\begin{bmatrix} xt1 & xt2* & xt3* & xt4 \\ xt2 & -x1* & xt4* & -xt3 \\ xt3 & xt4* & -xt1* & -xt2 \\ xt4 & -xt3* & -xt2* & xt1 \end{bmatrix}$$

Step 6*:* These encoded symbols are transferred over a MIMO Channel [30] [31] Matrix or H-Matrix, which can be mathematically represented as,

$$\boldsymbol{H}=\begin{bmatrix} hc11 & hc12 & hc13 & hc14 \\ hc21 & hc22 & hc23 & hc24 \\ hc31 & hc32 & hc33 & hc34 \\ hc41 & hc42 & hc43 & hc44 \end{bmatrix}$$

The input symbols associated with the above MIMO channel are affected by the noise until the said symbols reach the receivers. Additive White Gaussian noise is denoted by *ne*. The following expressions show the sequence of recipients in four slots as per following:

First slot:

$$\begin{bmatrix} yr11 \\ yr21 \\ yr31 \\ yr41 \end{bmatrix} = \begin{bmatrix} hc11 & hc12 & hc13 & hc14 \\ h21 & hc22 & hc23 & hc24 \\ h31 & hc32 & hc33 & hc34 \\ hc41 & h42 & hc43 & hc44 \end{bmatrix} * \begin{bmatrix} xt1 \\ xt2 \\ xt3 \\ xt4 \end{bmatrix} + \begin{bmatrix} ne11 \\ ne21 \\ ne31 \\ ne41 \end{bmatrix}$$

Second slot:

$$\begin{bmatrix} yr12 \\ yr22 \\ yr32 \\ yr42 \end{bmatrix} = \begin{bmatrix} hc11 & hc12 & hc13 & hc14 \\ hc21 & hc22 & hc23 & hc24 \\ hc31 & hc32 & hc33 & hc34 \\ hc41 & hc42 & hc43 & hc44 \end{bmatrix} * \begin{bmatrix} xt2* \\ -xt1* \\ xt4* \\ -xt3* \end{bmatrix} + \begin{bmatrix} ne12 \\ ne22 \\ ne32 \\ ne42 \end{bmatrix}$$

Third slot:

$$\begin{bmatrix} yr13 \\ yr23 \\ yr33 \\ yr43 \end{bmatrix} = \begin{bmatrix} hc11 & hc12 & hc13 & hc14 \\ hc21 & hc22 & hc23 & hc24 \\ hc31 & hc32 & hc33 & hc34 \\ hc41 & hc42 & hc43 & hc44 \end{bmatrix} * \begin{bmatrix} xt3* \\ xt4* \\ -xt1* \\ -xt2* \end{bmatrix} + \begin{bmatrix} ne13 \\ ne23 \\ ne33 \\ ne43 \end{bmatrix}$$

Fourth slot:

$$\begin{bmatrix} yr14 \\ yr24 \\ yr34 \\ yr44 \end{bmatrix} = \begin{bmatrix} hc11 & hc12 & hc13 & hc14 \\ hc21 & hc22 & hc23 & hc24 \\ hc31 & hc32 & hc33 & hc34 \\ hc41 & hc42 & hc43 & hc44 \end{bmatrix} * \begin{bmatrix} xt4 \\ -xt3 \\ -xt2 \\ -xt1 \end{bmatrix} + \begin{bmatrix} ne14 \\ ne24 \\ ne34 \\ ne44 \end{bmatrix}$$

The above equations in matrix form represent the receiver equations.

The receiver equations can also be represented in a matrix from in the following manner-

$$\begin{bmatrix} yr1 \\ yr2 \\ yr3 \\ yr4 \\ yr1* \\ yr2* \\ yr3* \\ yr4* \end{bmatrix} = \begin{bmatrix} hc1 & hc2 & hc3 & hc4 \\ hc2 & -hc1 & hc4 & -hc3 \\ hc3 & -hc4 & -hc1 & hc2 \\ hc4 & hc3 & -hc2 & -hc1 \\ hc1* & hc2* & hc3* & hc4* \\ hc2* & -hc1* & hc4* & -hc3* \\ hc3* & -hc4* & -hc1* & hc2* \\ hc4* & hc3* & -hc2* & -hc1* \end{bmatrix} * \begin{bmatrix} xt1 \\ xt2 \\ xt3 \\ xt4 \end{bmatrix} + \begin{bmatrix} ne1 \\ ne2 \\ ne3 \\ ne4 \\ ne1* \\ ne2* \\ ne3* \\ ne4* \end{bmatrix} \quad (5)$$

The above matrix is written as $yr = H_{ef}\, xt + ne$

The above matrix (5) is written in the form of equations in the following manner-

$$yr1 = hc1xt1 + hc2xt2 + hc3xt3 + hc4xt4 + ne1 \quad (6)$$
$$yr2 = hc2xt1 - hc1xt2 + hc4xt3 - hc3xt4 + ne2 \quad (7)$$
$$yr3 = hc3xt1 - hc4xt2 - hc1xt3 + hc2xt4 + ne3 \quad (8)$$
$$yr4 = hc4xt1 + hc3xt2 - hc2xt3 - hc1xt4 + ne4 \quad (9)$$
$$yr1* = hc1 * xt1 + hc2 * xt2 + hc3 * xt3 + hc4 * xt4 + ne1* \quad (10)$$
$$yr2* = hc2 * xt1 - hc1 * xt2 + hc4 * xt3 - hc3 * xt4 + ne2* \quad (11)$$
$$yr3* = hc3 * xt1 - hc4 * xt2 - hc1 * xt3 + hc2 * xt4 + ne3* \quad (12)$$
$$yr4* = hc4 * xt1 + hc3 * xt2 - hc2 * xt3 - hc1 * xt4 + ne4* \quad (13)$$

Decoding Process:

In the finder, a complete CSIR (channel for data creation) is obtained so that the Maximal Ratio Combining (MRC) process is used. MRC combines the selected coefficients corresponding to the same complex channel matrix [32] shown below:

$\tilde{x}t = H_{ef}^{H}\, yr$ which is also written in the following manner-

$$\begin{bmatrix} \widetilde{xt1} \\ \widetilde{xt2} \\ \widetilde{xt3} \\ \widetilde{xt4} \end{bmatrix} = \begin{bmatrix} hc1 & hc2 & hc3 & hc4 & hc1* & hc2* & hc3* & hc4* \\ hc2 & -hc1 & -hc4 & hc3 & hc2* & -hc1* & -hc4* & hc3* \\ hc3 & hc4 & -hc1 & -hc2 & hc3* & hc4* & -hc1* & -hc2* \\ hc4 & -hc3 & hc2 & -hc1 & hc4* & -hc3* & hc2* & -hc1* \end{bmatrix} * \begin{bmatrix} yr1 \\ yr2 \\ yr3 \\ yr4 \\ yr1* \\ yr2* \\ yr3* \\ yr4* \end{bmatrix} \quad (14)$$

The above matrix (14) can be written in the form of equations as per following-

$\widetilde{xt1}$=hc1yr1+hc2yr2+hc3yr3+hc4yr4+hc1*yr1*+hc2*yr2*
+ hc3*yr3*+hc4yr4* (15)

$\widetilde{xt2}$=hc2yr1-hc1yr2-hc4yr3+hc3yr4+hc2*yr1*-hc1*yr2*-
hc4*yr3+Hc3*yr4* (16)

$\widetilde{xt3}$ =hc3yr1+hc4yr2-hc1yr3-hc2yr4+hc3*yr1*+hc4*yr2*-
hc1*yr3*-hc2*yr4* (17)

$\widetilde{xt4}$=hc4yr1-hc3yr2+hc2yr3-hc1yr4+hc4*yr1*-hc3*yr2*+
hc2*yr3*-hc1*yr4* (18)

The above equations from (6)-(18) narrate the design of 4x4 STBC MIMO System.

6. Proposed model

The communication link model has been implemented using hardware co-simulation block. The description of the proposed model and the hardware design has been depicted in sections 6.1 and 6.2 respectively.

6.1. Description of the proposed model

In order to minimize BER and to increase SNR the following model shown in Fig.5 has been proposed for 5G communication for the tropical regions. This model has been designed using Xilinx System generator. The Bernoulli binary generator generates samples as a vector output. The samples pass through the unbuffer block which converts a frame to scalar samples output at a higher rate. The input samples then pass through the 'Gateway In' block. This block converts the inputs of different types of Simulink integers to Xilinx fixed-point data. Then the data goes through 'Gateway Out'. This block converts Xilinx fixed point inputs into outputs of Simulink integers. The output data now passes through the buffer block. The buffer converts scalar samples to a frame output at a lower rate. The input samples now pass through the TCM encoder designed for tropical regions. An automatic gain controller (AGC) is added in the TCM encoder. This encoder convolutionally encodes binary data and modulates using the phase shift keying method. This encoder is designed in such a way that when signal passes through this encoder the signal power remains high. Then the input data passes through OSTBC encoder which is devised for tropical regions. This encoder encodes the input message using an orthogonal space-time block code (OSTBC). The OSTBC comprises rate 1 for 2 transmit antennas, rate 1/2 or 3/4 for 3 and 4 transmit antennas. This encoder is designed in such a way that when input message passes through this encoder then its SNR remains high. The input signal now passes through MIMO channel. The MIMO channel filters input signal through a MIMO multipath fading channel. In the MIMO channel there

are included two types of fading channels viz. Rayleigh fading and Rician fading. From MIMO channel the signal passes through the rain attenuation channel. When a signal passes through this rain attenuation channel, the signal gets attenuated. Now this input signal makes its way through the OSTBC combiner. This combiner combines the received signal and channel estimate inputs in accordance with the structure of the orthogonal space-time block code (OSTBC). This combiner is drawn in such a manner that when the input signal goes through this combiner, the signal power gets enhanced. Therefore, the input signal moves along TCM decoder. This decoder uses the Viterbi algorithm to decode trellis-coded modulation data, modulated using the phase shift keying modulation method. Thereafter the input signal travels along the error rate calculation which computes the error rate of the received data by comparing it to a delayed version of the transmitted data. The block output is a three-element vector consisting of error rate, followed by the number of errors detected and the total number of symbols compared. This vector can be sent to either the workspace or an output port.

The values of BER relies on a number of parameters like no. of samples per frame, no of transmitting antennas in the transmitter and no of receiving antennas in the receiver. The BER values also depend on types of fading distribution.

Table 1: Change of BER due to various parameters

Parameters			
No of samples per frame	**No of transmitting antennas**	**No of receiving antennas**	**BER**
600	2	2	0.4567
1200	2	2	0.4225
1500	2	2	0.4223
1800	2	2	0.4167
2700	2	2	0.4122
3000	2	2	0.4093
600	3	3	0.4483
1200	3	3	0.415
1500	3	3	0.4173
1800	3	3	0.4122
2700	3	3	0.4093
3000	3	3	0.406
600	4	4	0.4517
1200	4	4	0.4158
1500	4	4	0.4193
1800	4	4	0.4111
2700	4	4	0.4059
3000	4	4	0.4033

Table 2: Change of BER due to fading distribution

Parameters		
No of samples per frame	**Type of fading distribution**	**BER**
600	Rayleigh	0.4483
1200	Rayleigh	0.415
1500	Rayleigh	0.4173
1800	Rayleigh	0.4122
2700	Rayleigh	0.4093
3000	Rayleigh	0.406
600	Rician	0.466
1200	Rician	0.4242
1500	Rician	0.4247
1800	Rician	0.4178
2700	Rician	0.413
3000	Rician	0.4093

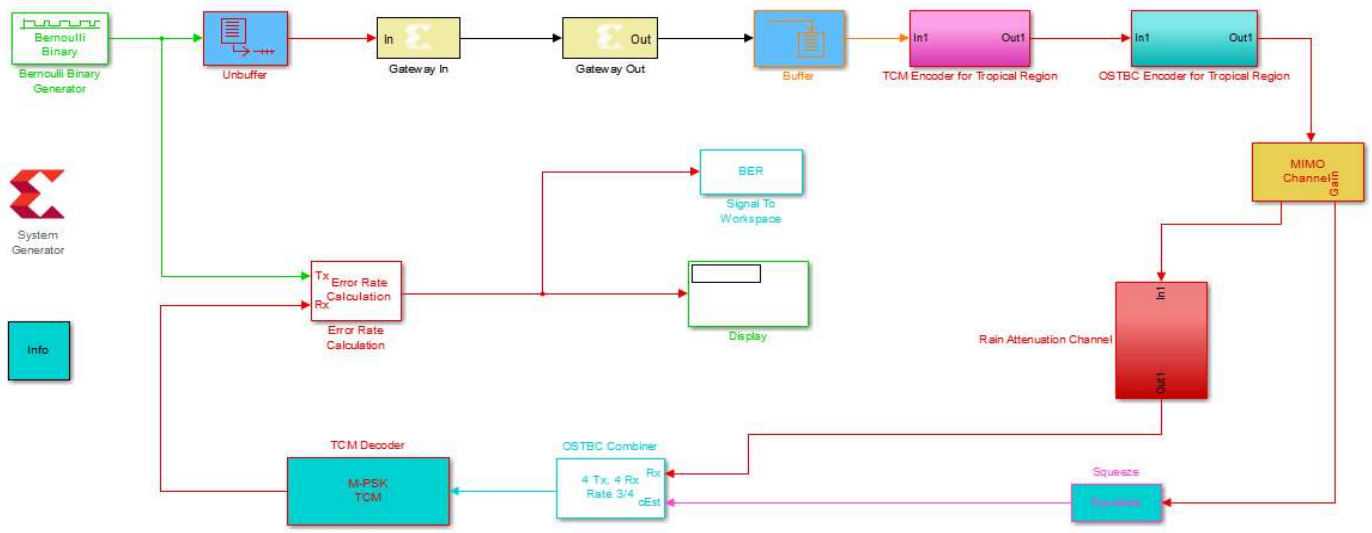

Fig.5: Communication link model for 5G communication using system generator

Hence by applying equations (6)-(13) and (15)-(18) the 4x4 OSTBC MIMO System used in the proposed communication link model has been designed using system generator and it is displayed in Fig. 6 given below. This OSTBC MIMO system is much effective in the tropical regions because it reduces signal attenuation and enhances BER of the signal. This OSTBC MIMO System has been reflected in the communication link model for 5G Communication using system generator demonstrated in Figure 5.

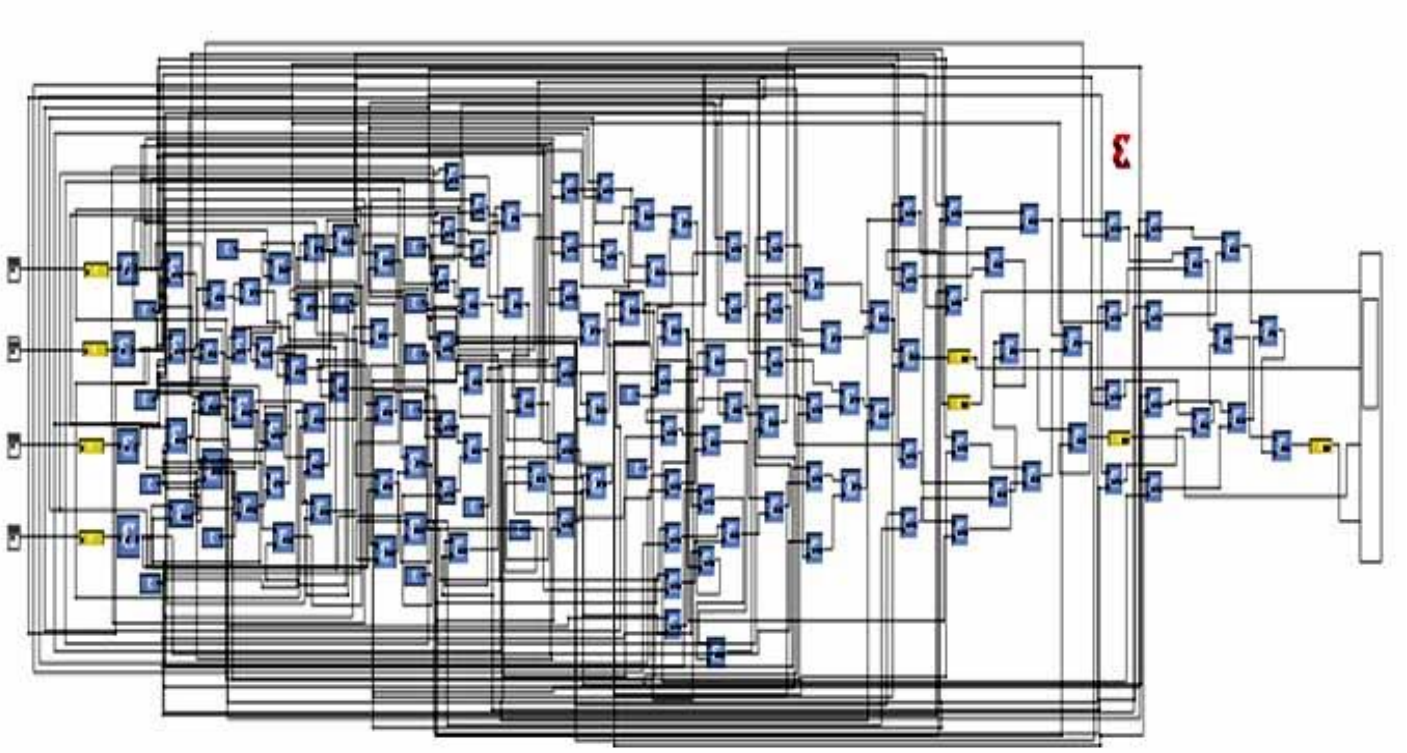

Fig 6: Model of 4X4 OSTBC MIMO System using system generator

6.2. Hardware design of the proposed model

The proposed communication link model comprising 4x4 OSTBC MIMO has been implemented in Xilinx kintex-7. The hardware design of the proposed communication link model containing 4x4 OSTBC MIMO systems is displayed in Figs. (7) - (12)**.**The HDL code has been employed to implement the models. The RTL Schematic, top level RTL Schematic, Schematic view, designed model using FPGA editor, device utilization summary have been tabulated below in table 3. In table3 utilization of resources as displayed appears much less. Results for low cost and low power System on Chip (SoC) in consequence with a 4x4 OSTBC MIMO has been designed as highlighted in tables 3 and 4..Maximum delay of the clock is 1.231000 ns and net skew is 0.135000 ns.

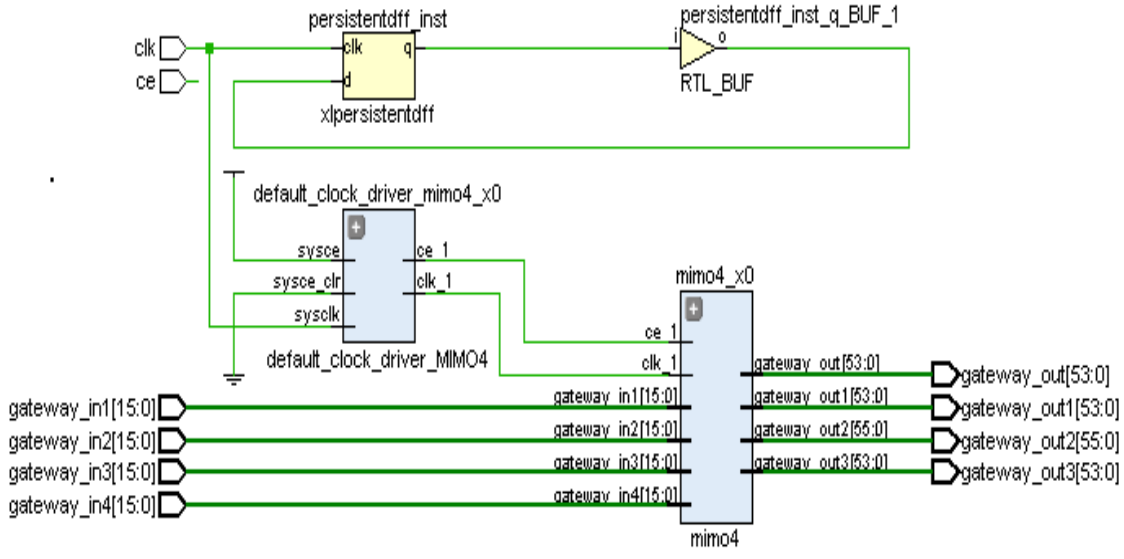

Fig 7: RTL Schematic of 4x4 OSTBC MIMO

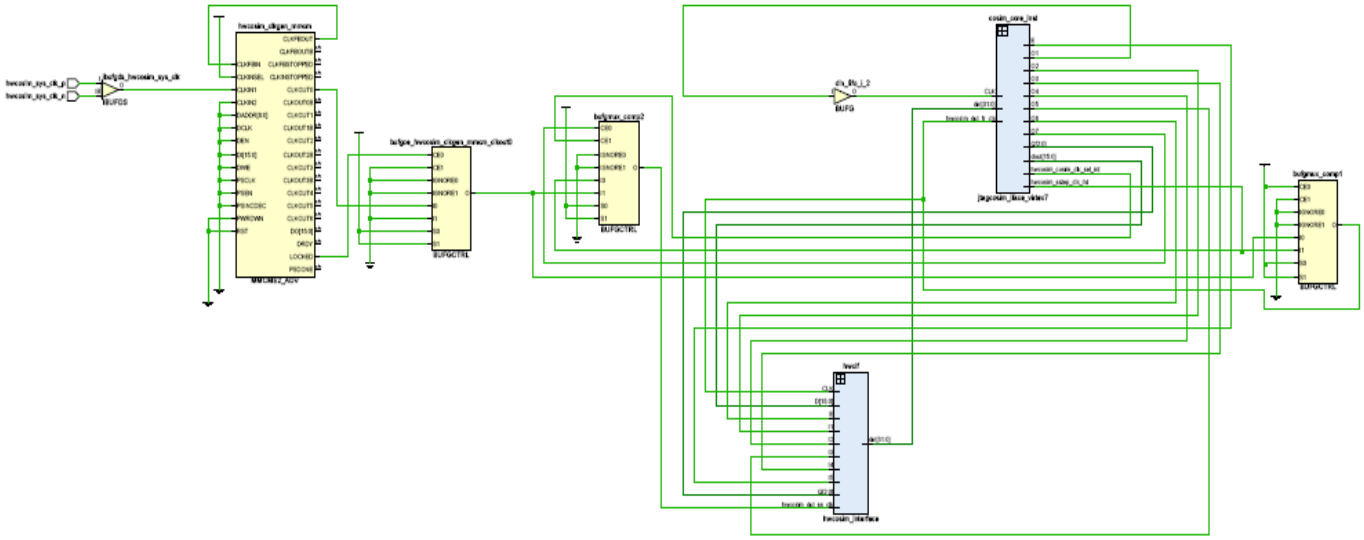

Fig 8: Technology Schematic view of 4x4 OSTBC MIMO

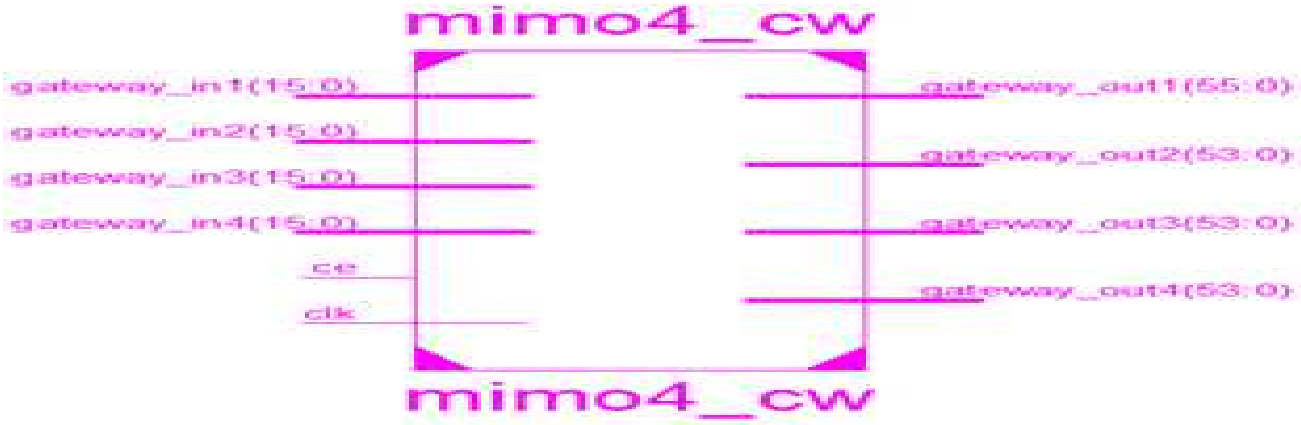

Fig 9: Top level RTL Schematic of 4x4 OSTBC MIMO

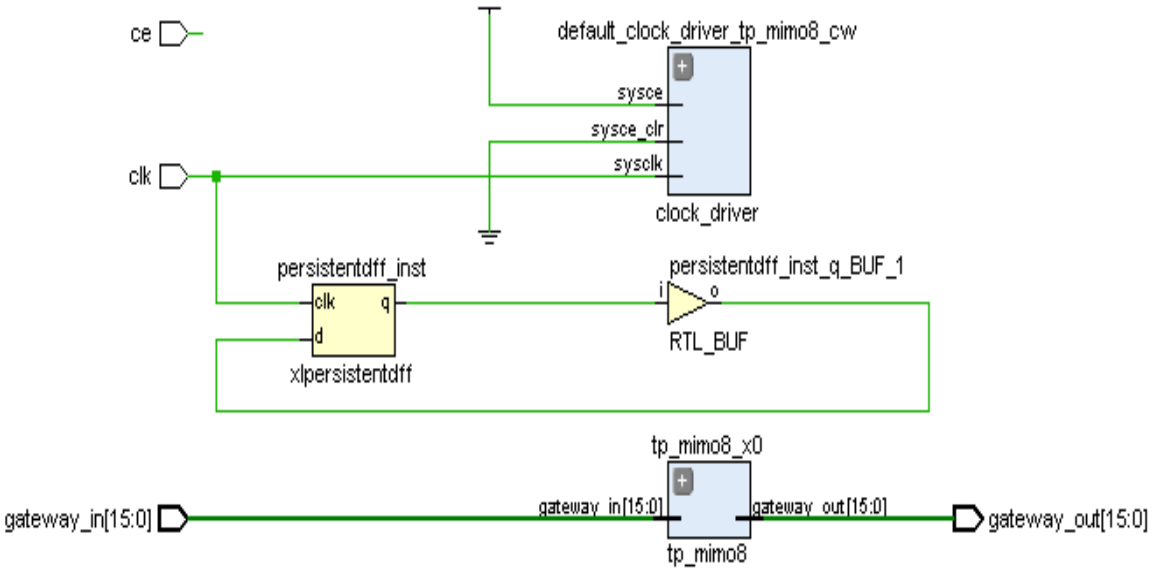

Fig 10: RTL Schematic of communication link model

Fig 11: Top level RTL Schematic of communication link model

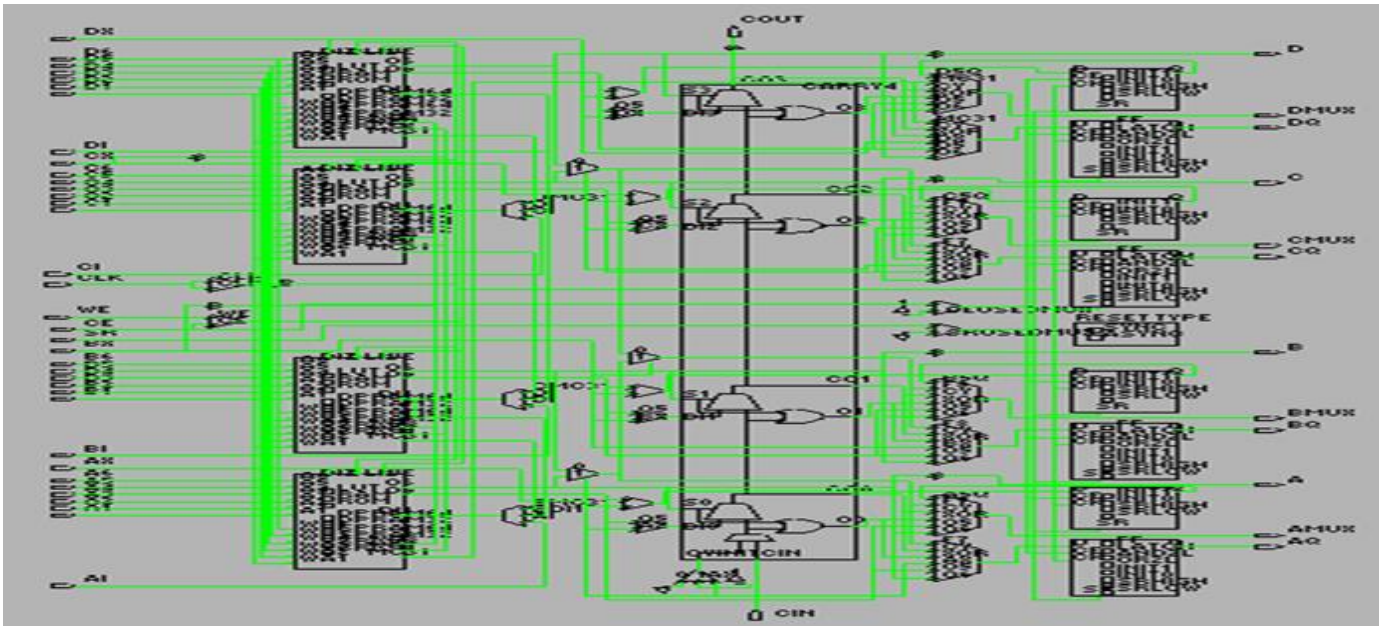

Fig 12: Model of 4x4 OSTBC MIMO using FPGA editor

Table 3: Device utilization summary for Xilinx Kintex 7FPGA Kit

Resources	Utilization	Available	Utilization %
Slice LUTs	2776	203800	1.36
Slice Registers	518	407600	0.13
Memory	2	445	0.45
DSP	33	840	3.93
IO	2	500	0.40
Clocking	4	32	12.50

Table 4: Power Analysis of 4x4 OSTBC MIMO

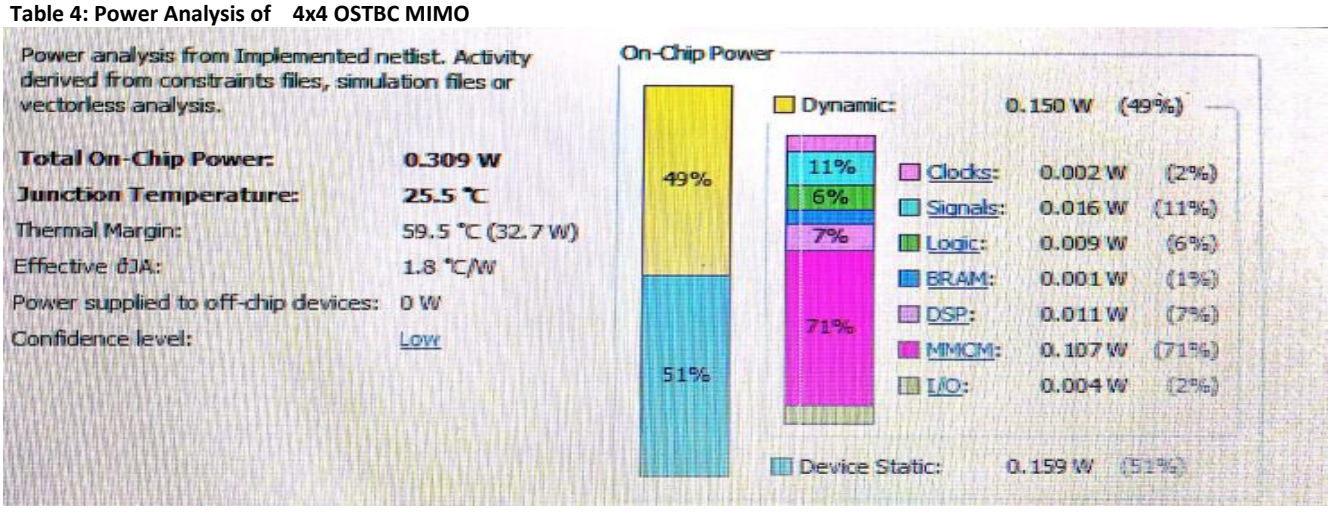

7. Result analysis and discussion

The result of the overall work of the proposed model has been analyzed in this paper. It reveals that the analysis of result provides two parts-simulation part and synthesis part. After synthesis the reconfigurable block has been implemented using Xilinx Kintex7 FPGA board and its device Utilization is shown in Table 3.In sec 7.1, the result of the simulation part has been reflected and in sec 7.2, synthesis part has been demonstrated. In the synthesis portion timely behavioral analysis is important for two purposes. Firstly, it is inevitable to verify the connection between two connectors whether the cycle used meets all the time requirements so that all the events are produced within the required time expected by the regional environment. Secondly, for integrating digital circuits, the delays are determined within which the output events must be produced. While the proposed model is simulated, the values of BER are exhibited on the display block of the model for Rayleigh fading distribution and Rician fading distribution. Hence the BER values have been compared with two different types of fading distributions and this phenomenon has been demonstrated in Fig. 13. Different types of MIMO techniques (2x2, 3x3 and 4x4) have been applied to this proposed model. The BER values for different MIMO techniques have been displayed on the display block of this model and the comparison of BER for different MIMO techniques have been plotted in Fig.14. In the figures 15 to 17, the synthesis part of the result illustrates the hardware data sheet of encoder, digital clock manager, and multiple clocks. In the figures 18 to 21 the same result depicts the hardware data sheet of timing diagram for encoder, digital clock manager and multiple clocks respectively.

7.1 Simulation Result

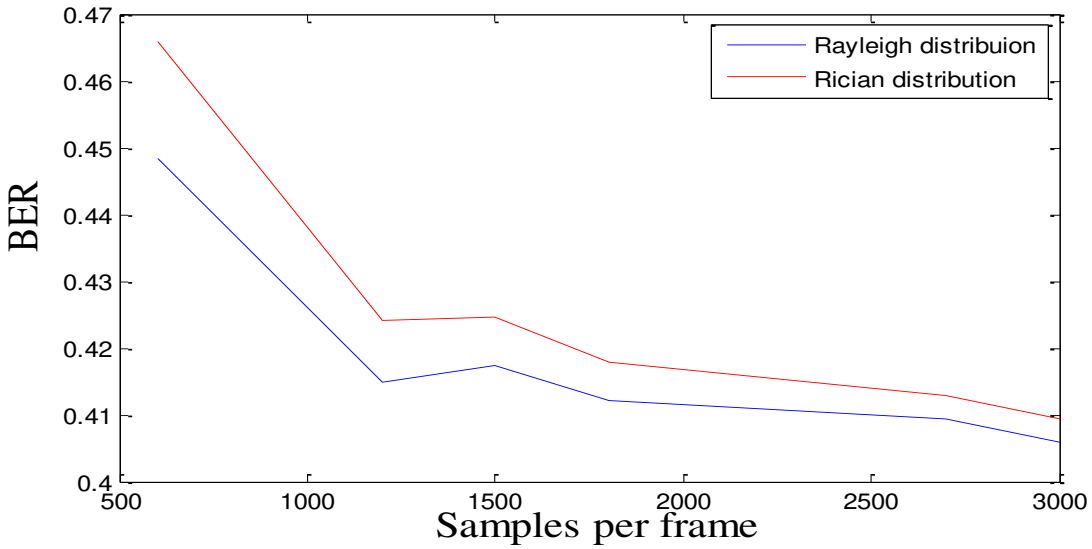

Fig. 13: Comparison of BER between Rayleigh fading distribution and Rician fading distribution

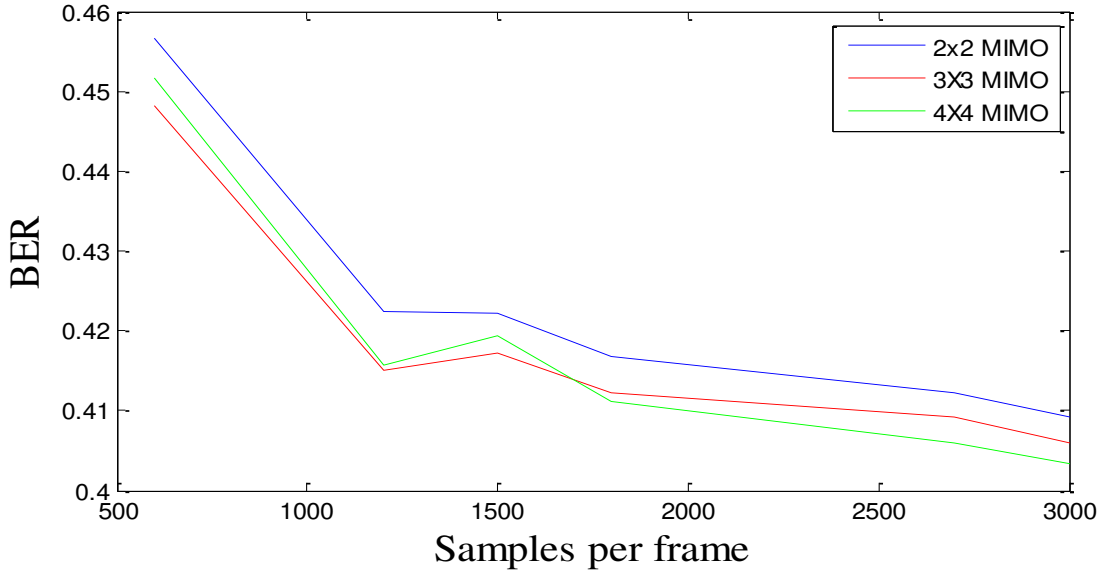

Fig 14: Comparison of BER for different MIMO techniques

7.2 **Synthesis Result:**

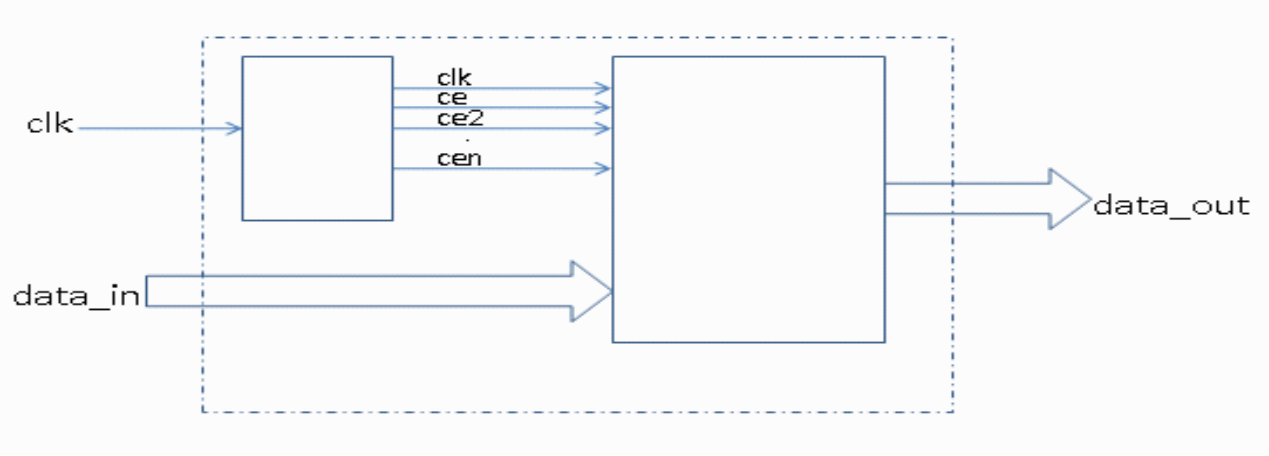

Fig. 15: Hardware data sheet for design of Encoder

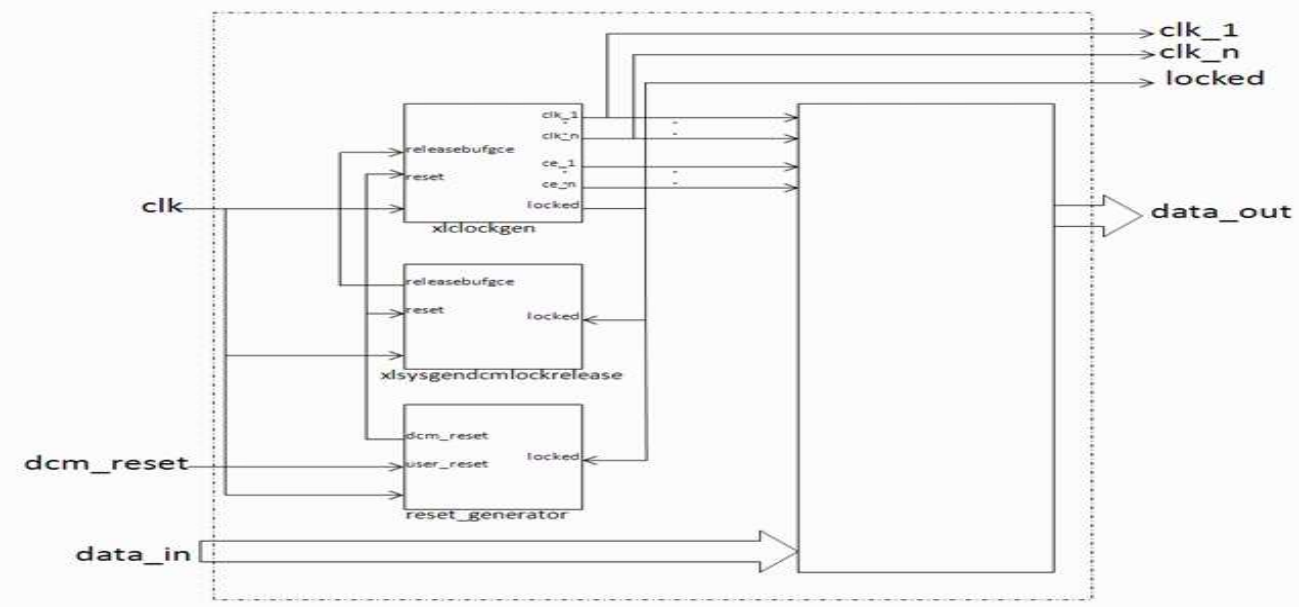

Fig 16*:* Hardware data sheet for design of Digital clock manager

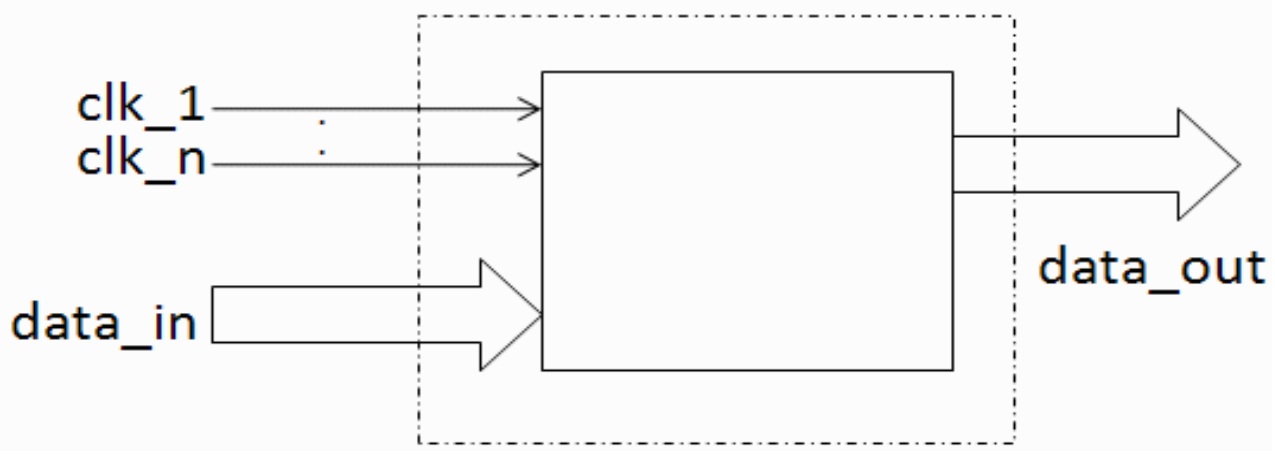

Fig. 17: *Hardware data sheet for design of multiple clocks*

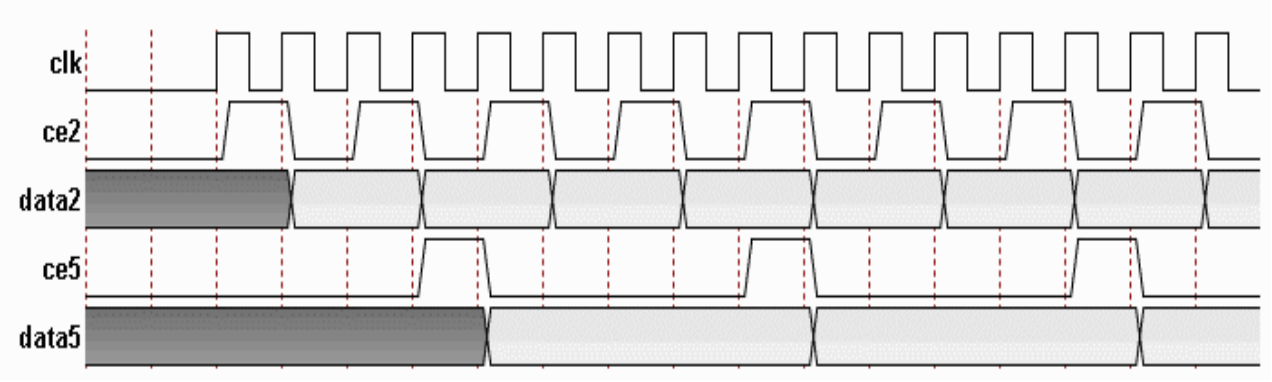

Fig. 18: Hardware data sheet of timing diagram

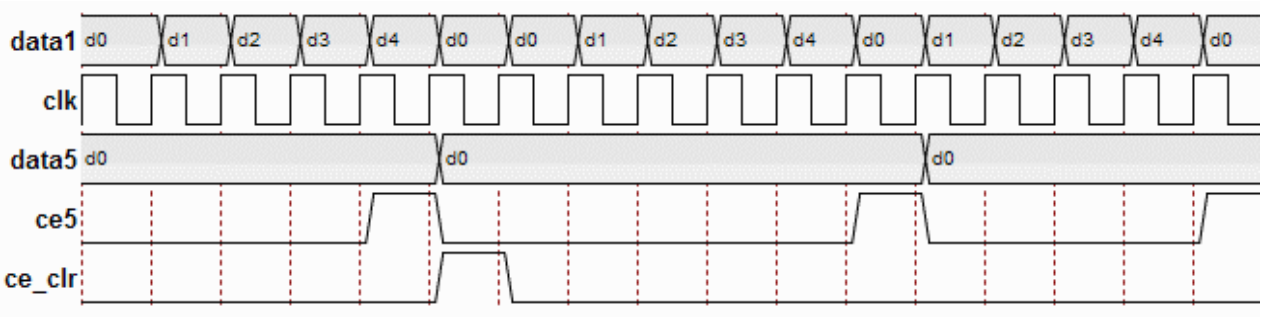

Fig.19: Hardware data sheet of timing diagram for Encoder

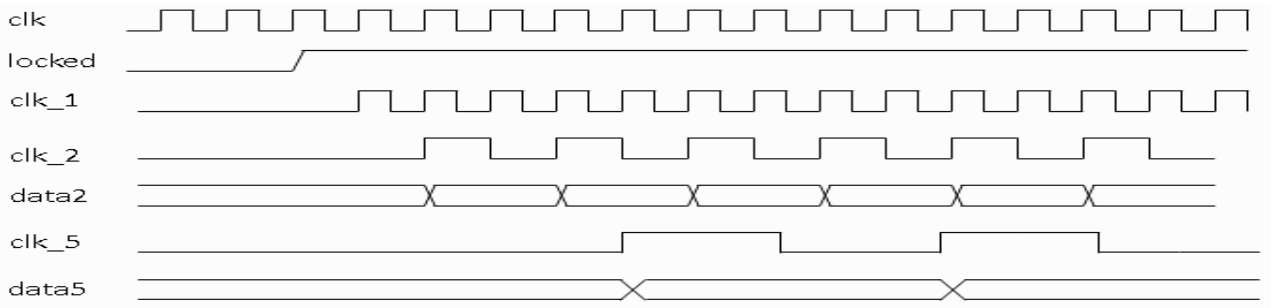

Fig. 20: Hardware data sheet of timing diagram for digital clock manager

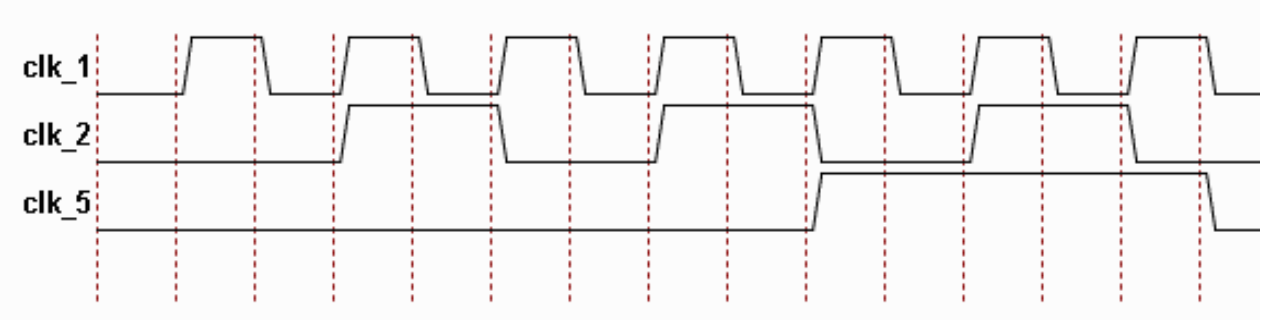

Fig. 21: Hardware data sheet of timing diagram for multiple clocks

8. Conclusion

In this paper this proposed model has been designed especially for the tropical regions. This model will satisfy the long cherished desire of the people of tropical regions in respect of wireless communication. This proposed model has been depicted in order to maintain minimum BER in the tropical regions. From figure 13 it is observed that Rayleigh distribution has provided the minimum bit error rate (BER) than that of Rician distribution. From figure 14 it would transpire that 4x4 MIMO technique has produced the better result than that of 2x2 and 3x3 MIMO techniques. In other words, by using 4x4 MIMO techniques the signal to noise ratio (SNR) increases in the tropical regions. For this enhancement of SNR the distortion of signal becomes much less if any major message is transmitted from a transmitter to a receiver. In the figures 15 to 21 the synthesis results of the communication link model have been reflected. The designed hardware model of 4x4 OSTBC MIMO System produces low cost and low power as shown in table 3, table 4 and it will be a very effective model for tropical regions for reducing signal attenuation. From the overall work performed in this paper it is concluded that the using of this proposed model will bring down the cost, power and increase the reliability of the system than that of using other models. As a result, this proposed model will be easily accessible to any user of the tropical regions.

Abbreviations
TCM: Trellis coded modulation; SNR: Signal-to-noise ratio; STBC: Space time block coding; OSTBC: Orthogonal space- time block code; QOSTBC: Quasi orthogonal space time block code; BER: Bit error rate; MIMO: Multi input-multi output; AGC: Automatic gain controller

Authors' contributions
Both the authors have contributed their efforts to write the entire manuscript. The authors read and approved the final manuscript.

Funding
No funding support. Personal funding will be provided.

Availability of data and materials
No data are necessary in this paper.

Competing interests
Authors have no financial or non-financial competing interests in this regard

.

References

1. T.S. Rappaport, *et al:* ``Millimeter wave mobile communications for 5G cellular: It will work!" *IEEE Access*, vol. 1, pp. 335-349(2013).
2. Z.Yun and M.F. Iskander.: ``Ray tracing for radio propagation modeling: Principles and applications," *IEEE Access*, vol. 3, pp. 1089-1100(2015).
3. J. C. Aviles and A. Kouki: ``Exploiting site-specific propagation characteristics in directional search at 28 GHz," *IEEE Access*, vol. 4, pp.3894-3906(2016).
4. A.N.Krasiloy, M.V.Susloparov, O.O.Filatov et.al. ``Performance Evaluation of TCP Data Transmission in 5G mm Wave Networks" *J. Commun. Technol. Electron.* **65,** 735–740 (2020)
5. X. Li, X. Yang, L. Li, J. Jin ,N. Zhao and C. Zhang : ``Performance analysis of distributed MIMO with ZF receivers over semi-correlated K fading channels," *IEEE Access*, vol. 5, pp. 9291-9303(2017).
6. C. Sanchis, M.-T. Martínez-Ingles, J.-M. Molina-García-Pardo, J. Pascual-García, and J.-V. Rodríguez: ``Experimental study of MIMO-OFDM transmissions at 94 GHz in indoor environments," *IEEE Access*, vol. 5, pp. 7488-7494(2017).
7. A. Paulraj, et al.: "An overview of mimo communications - a key to gigabit wireless," Proceedings of the IEEE, vol. 92, no. 2, pp. 198–218(2004).
8. A.F. Molisch, et al.: "Capacity of MIMO systems based on measured wireless channels," IEEE Journal on Selected Areas in Communications, vol. 20, no. 3, pp. 561–569(2002).
9. S. Geng, N. Fan: "28 GHz MIMO Channel Characteristics Analysis for 5G Communication Systems, 5GWN. ISBN: 978-3-31972-822-3(2017).
10. Y. Huo, X. Dong and W. Xu: ``5G Cellular User Equipment: From Theory to Practical Hardware Design" IEEE Access, vol-5, pp. 13992-14010(2017).
11. Z. Albataineh, K. Hayajneh, H.B.Salameh, C. Dang and A. Dagmesh: "Robust massive MIMO channel estimation for 5G networks using compressive sensing technique", International Journal of Electronics and Communications, vol-120, pp.153197-153203(2020).
12. D. Divsalar and M. K. Simon: "The Design of Trellis Coded MPSK for Fading Channels: Performance Criteria", *IEEE Trans. on Commun.* Vol. 36, No. 9, pp. 1004–1011(1988).
13. *Specific Attenuation Model for Rain for Use in Prediction Methods*, document ITU-R P.838-3, (2005).
14. J. S. Mandeep, Y. N. Ng, H. Abdullah and. M. Abdullah: ``The study of rain specific attenuation for the prediction of satellite propagation in Malaysia," *J. Infr., Millim., Terahertz Waves*, vol. 31, no. 6, pp. 681-689(2010).
15. H. Y. Lam, L. Luini, J. Din, M. J. Alhilali, S. Jong, and F. Land Cuervo: ``Impact of rain attenuation on 5G millimeter wave communication Systems in equatorial Malaysia investigated through disdrometer data", in *Proc. 11th Eur. Conf. Antennas Propag.(EUCAP)*, pp. 1793- 1797(2017).
16. S. Shrestha and D.-Y. Cho: ``Rain attenuation over terrestrial microwave links in South Korea," *IET Microw., Antennas Propag.*, vol. 11, no. 7, pp. 1031-1039(2017).
17. P. Thorvaldsen and I. Henne: ``Outdoor transmission measurement at 26 GHz; results of a 4 years trial in Prague," in *Proc. 1st URSI Atlantic Radio Sci. Conf. (URSI AT-RASC)*, pp. 1-9(2015).
18. L. D. S. Mello, M.S. Pontes and E. C. D. Miranda, ``Measurements and prediction of outage intensity owing to rain attenuation," *Electron. Lett.* vol. 48, no. 10, pp. 545-546(2012).
19. F. Moupfouma: ``Electromagnetic waves attenuation due to rain: A prediction model for terrestrial or L.O.S SHF and EHF radio communication links," *J. Infr., Millim., Terahertz Waves*, vol. 30, no. 6, pp. 622-632(2009).
20. Propagation Data and Prediction Methods Required for the design of Earth-Space Telecommunication Systems, document Rec. ITU-R P.12- 618, pp. 1-27(2015).
21. *Propagation Data and Prediction Methods Required for the Design of Terrestrial Line-of-Sight Systems*, document ITU-R P.530-16(2015).
22. K. Ulaganathen, T.A. Rahman, A. Abdulrahman and S. K. B. A. Rahim, ``Comparative studies of the rain attenuation predictions for tropical regions," *Prog. Electromagn. Res. M*, April 2011, vol. 18, pp. 17-30.
23. M. Singh and J.E. Allnutt: ``Rain attenuation predictions at Ku-band in South East Asia countries," *Prog. Electromagn. Res.*, vol. 76, pp. 65-74(2007).
24. L. A. R. Da. Silva Mello, M.S. Pontes, R.M. De Souza, and N.A.P. Garcia: ``Prediction of rain attenuation in terrestrial links using full rainfall rate distribution'', *Electron. Lett.* vol. 43, no. 25, pp. 1442-1443(2007).
25. A.Y. Abdulrahman, T.A. Rahman, S.K.A. Rahim, and M.R.U. Islam : "Empirically derived path reduction factor for terrestrial microwave links operating at 15 Ghz in Peninsula Malaysia," *J. Electromagn.Waves Appl.*, vol. 25, no. 1, pp. 23-37(2011).
26. S.H. Lin: ``11-GHz radio: Nationwide long-term rain rate statistics and empirical calculation of 11-GHz microwave rain attenuation," *Bell Labs Tech. J.*, vol. 56, no. 9, pp. 1581-1604(1977).
27. L. F. Wei, L. F.: "Trellis-coded modulation with multidimensional constellations," IEEE Transactions on Information Theory, vol. 33, no. 4, pp.483– 501(1987).
28. G. Ungerboeck: "Channel coding with multilevel/phase signals," IEEE Transactions on Information Theory, vol. IT-28, no. 1, pp. 55 – 67(1982).
29. F. Christoph, Mecklenbräuker and Markus Rupp.: "Generalized Alamouti codes for trading quality of service against data rate in MIMO UMTS." EURASIP Journal on Applied Signal Processing 2004: 662-675(2004).
30. P. Carlos, P. Yannis, V. Rodolphe and C. Pierre, "Sensitivity of the MIMO Channel Characterization to the Modeling of the Environment", IEEE Transactions on Antennas and Propagation, Vol. 57, Issue 4, pp 1218-1227(2009).
31. A.F. Molisch: "A Generic Model for MIMO Wireless Propagation Channels in Macro- and Microcells" IEEE Transactions on Signal Processing, Vol. 52, Issue 1, pp 61-71(2004).
32. S.M. Alamouti: "A simple transmit diversity technique for wireless communications," *IEEE Journal Selected Areas Commun*., vol. 16, no. 8, pp. 1451-1458(1998).

Figure title and legend

Fig 1: Flowchart of the proposed communication kink model
Fig.2. Rain impact on electromagnetic wave propagation
Fig.3. A simple Trellis Code Modulation
Fig.4. MIMO Channel of 4x4 STBC Systems
Fig.5: Communication link model for 5G communication using system generator
Fig 6: Model of 4X4 OSTBC MIMO System using system generator
Fig 7: RTL Schematic of 4x4 OSTBC MIMO
Fig 8: Technology Schematic view of 4x4 OSTBC MIMO
Fig 9: Top level RTL Schematic of 4x4 OSTBC MIMO
Fig 10*:* RTL Schematic of communication link model
Fig 11: Top level RTL Schematic of communication link model
Fig 12: Model of 4x4 OSTBC MIMO using FPGA editor
Fig. 13: Comparison of BER between Rayleigh fading distribution and Rician fading distribution
Fig 14: Comparison of BER for different MIMO techniques
Fig. 15: Hardware data sheet for design of Encoder
Fig 16*:* Hardware data sheet for design of Digital clock manager
Fig. 17: *Hardware data sheet for design of multiple clocks*
Fig. 18: Hardware data sheet of timing diagram
Fig.19: Hardware data sheet of timing diagram for Encoder
Fig. 20: Hardware data sheet of timing diagram for digital clock manager
Fig. 21: Hardware data sheet of timing diagram for multiple clocks

Figures

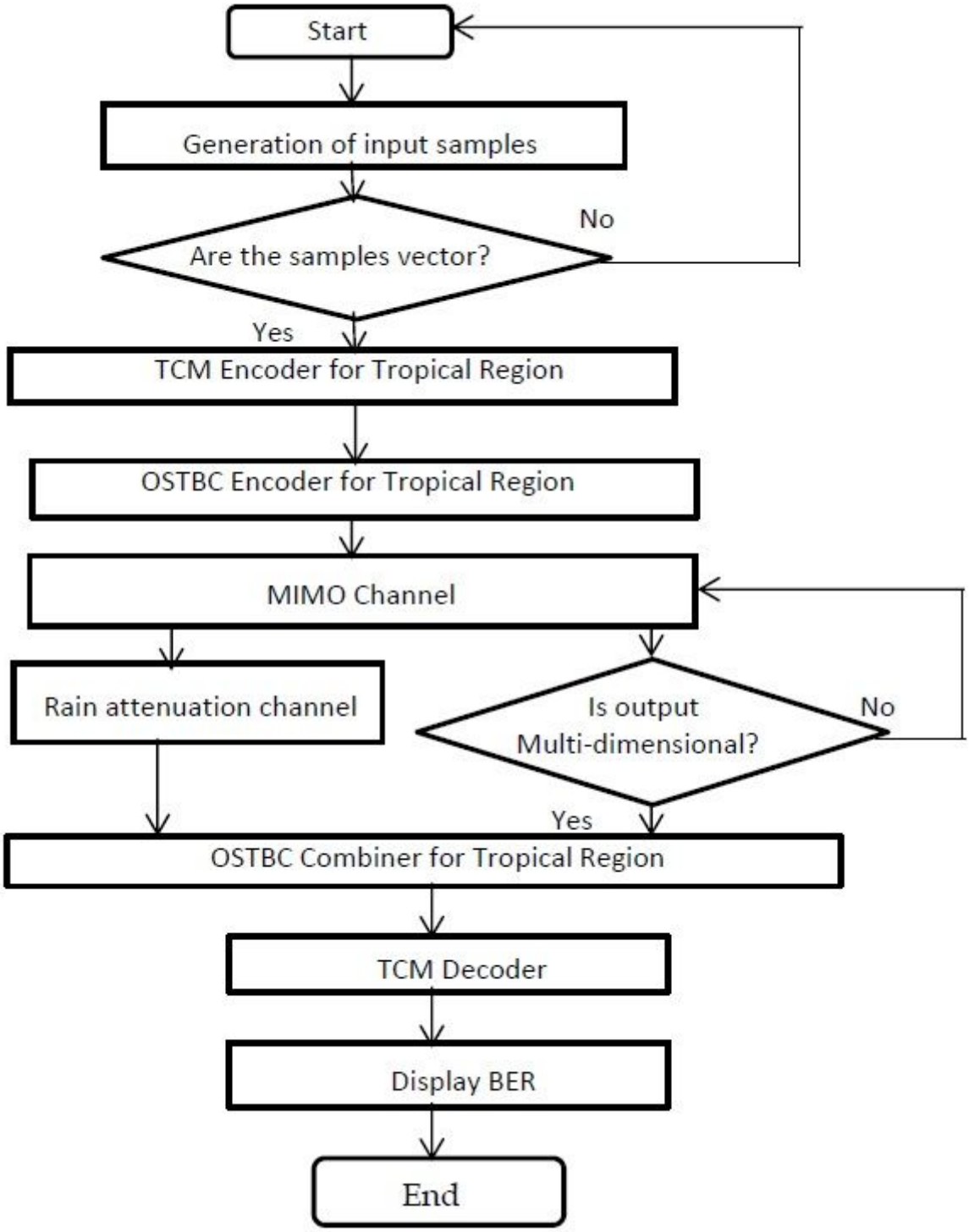

Figure 1

Flowchart of the proposed communication kink model

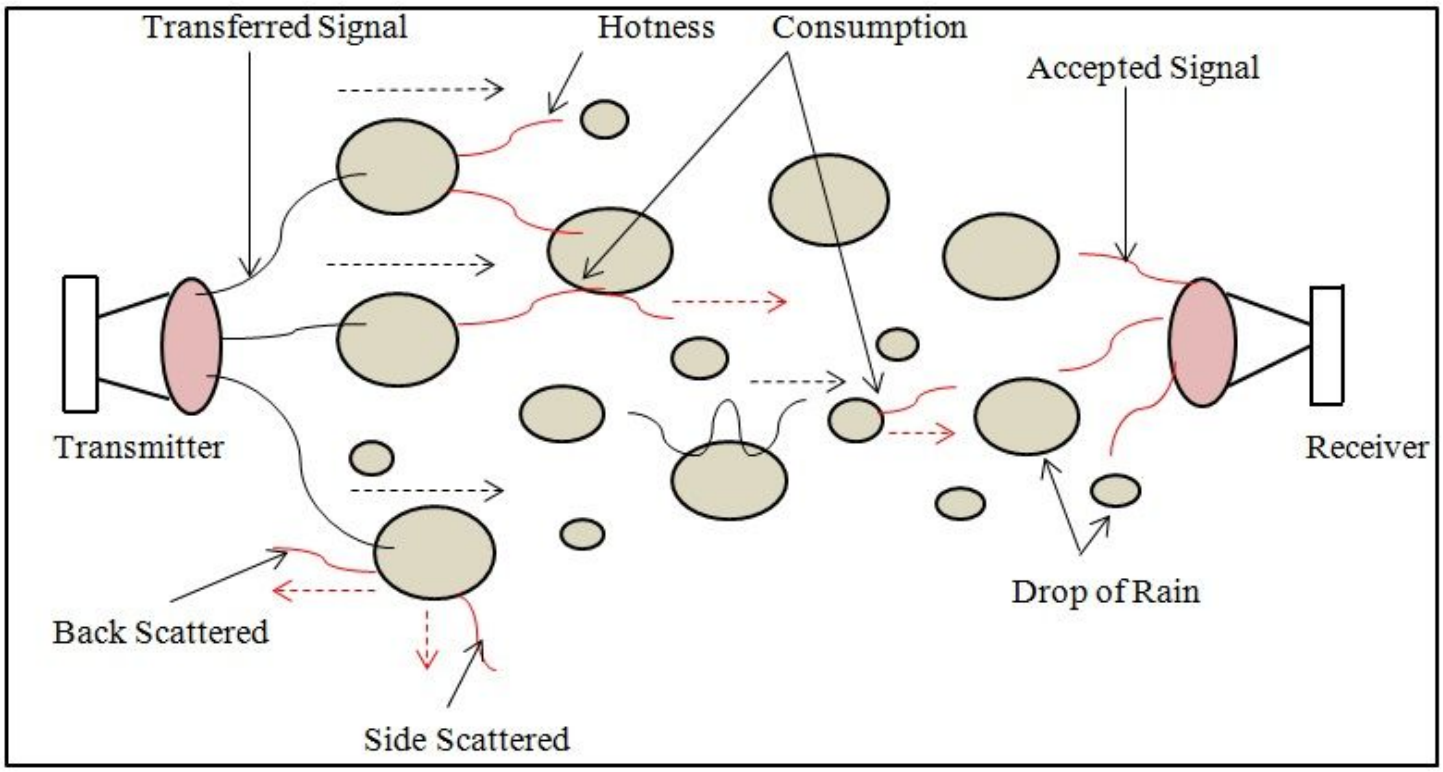

Figure 2

Rain impact on electromagnetic wave propagation

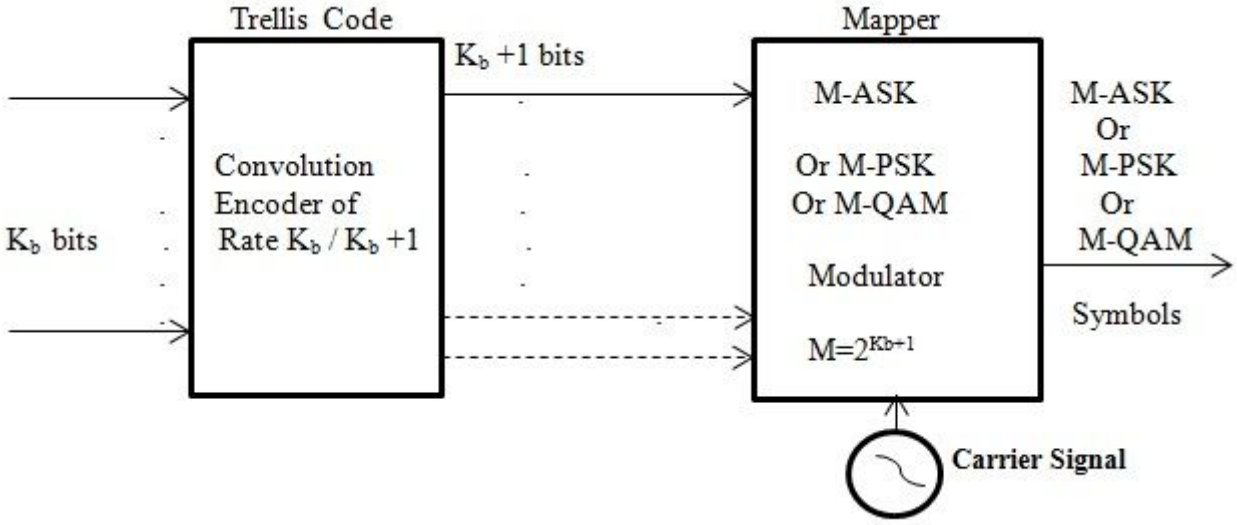

Figure 3

A simple Trellis Code Modulation

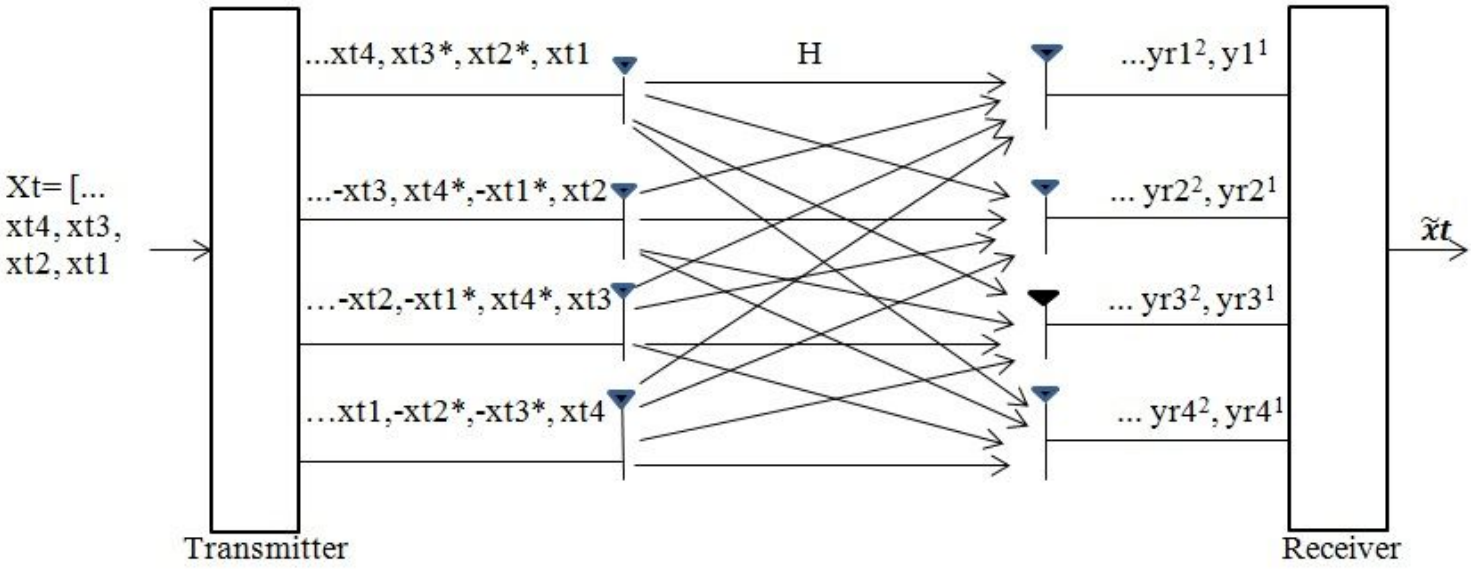

Figure 4

MIMO Channel of 4x4 STBC Systems

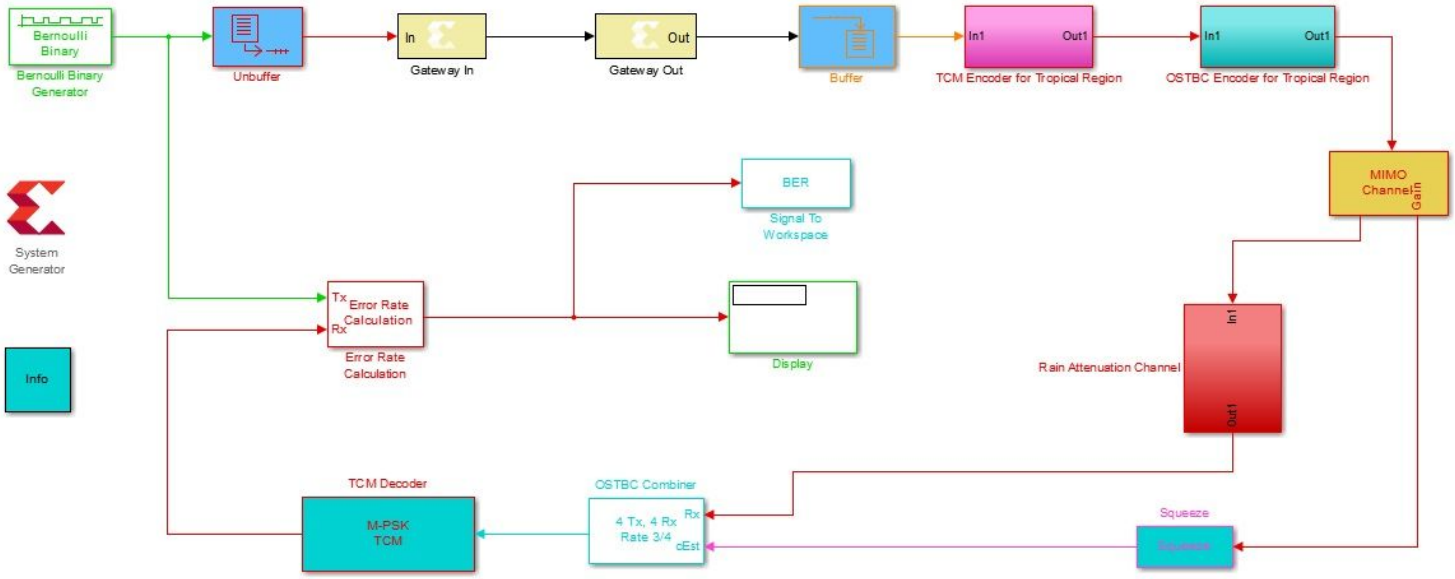

Figure 5

Communication link model for 5G communication using system generator

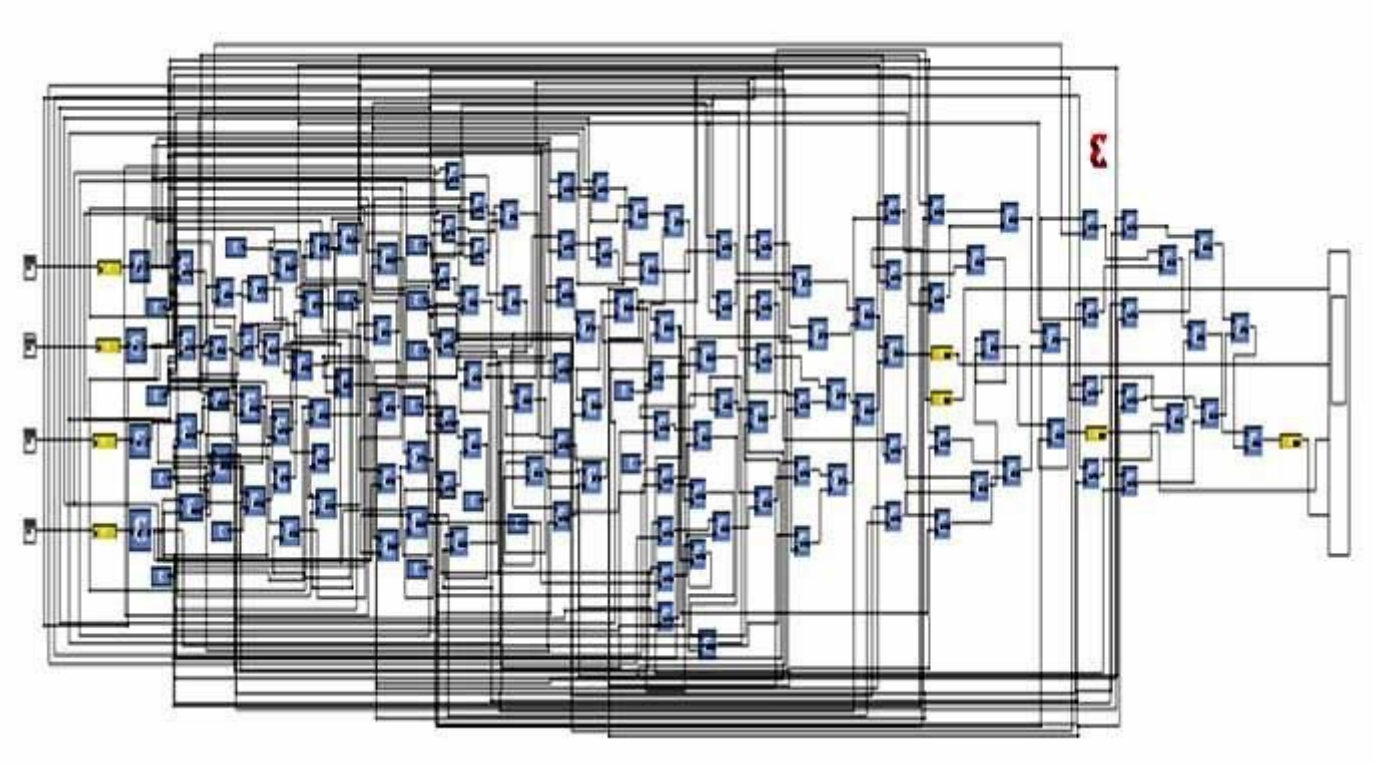

Figure 6

Model of 4X4 OSTBC MIMO System using system generator

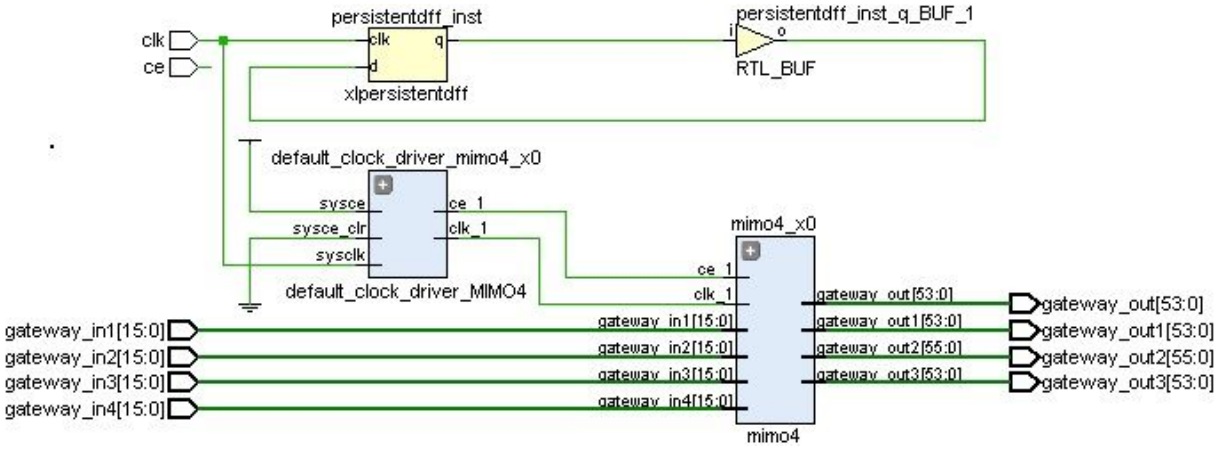

Figure 7

RTL Schematic of 4x4 OSTBC MIMO

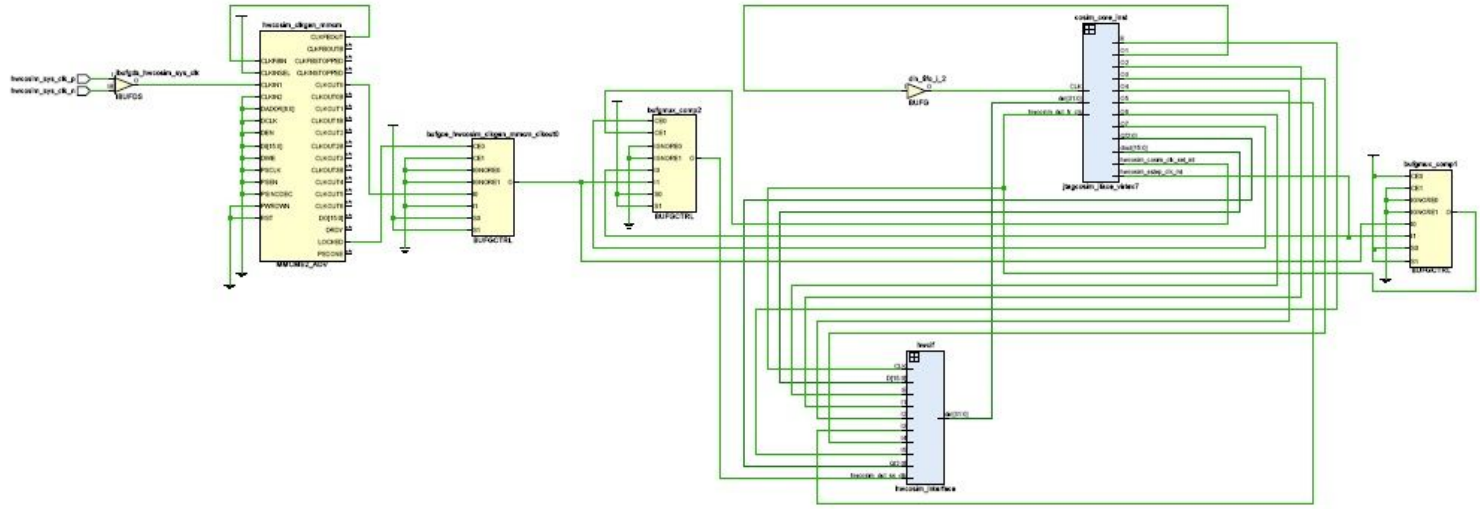

Figure 8

Technology Schematic view of 4x4 OSTBC MIMO

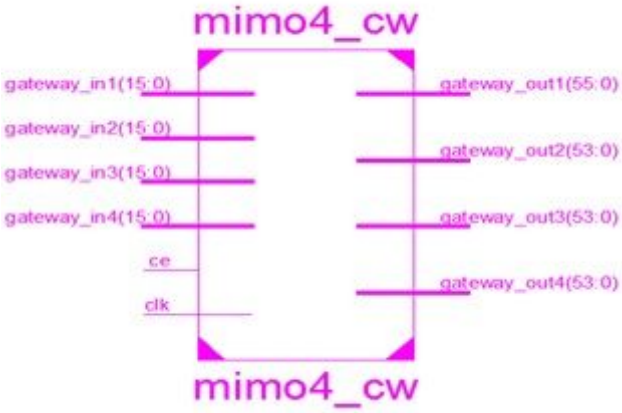

Figure 9

Top level RTL Schematic of 4x4 OSTBC MIMO

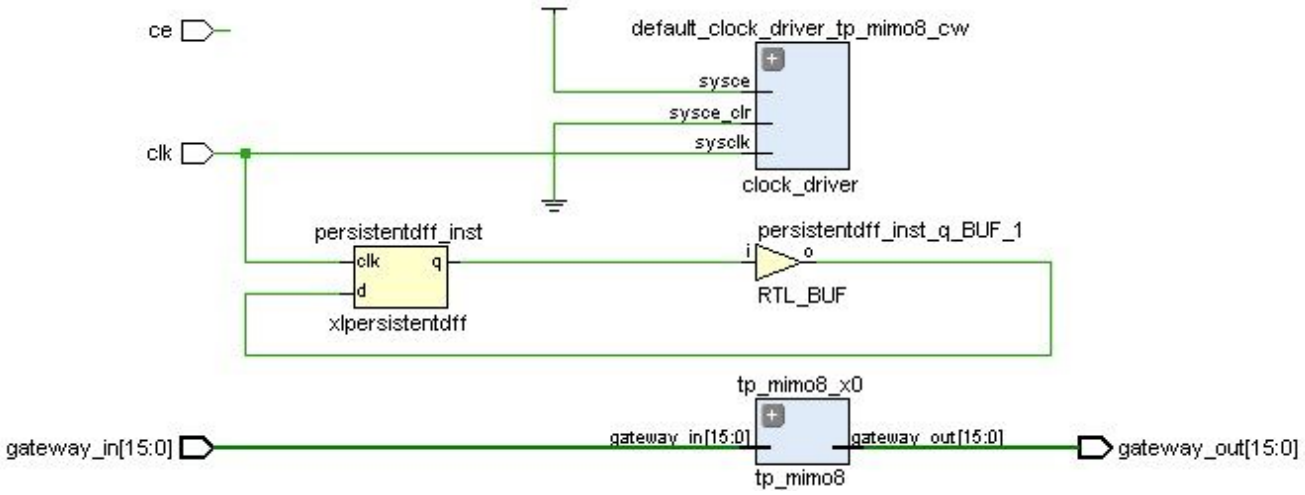

Figure 10

RTL Schematic of communication link model

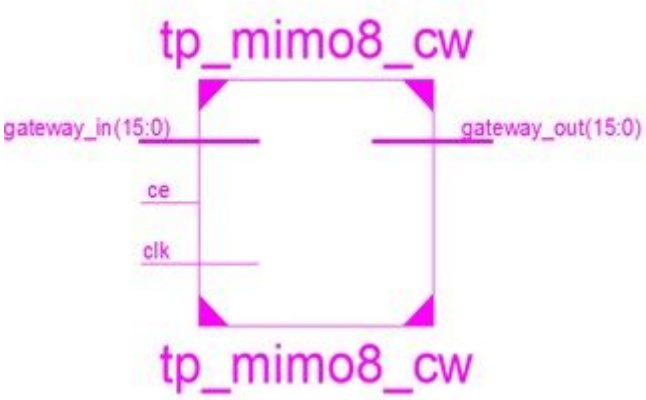

Figure 11

Top level RTL Schematic of communication link model

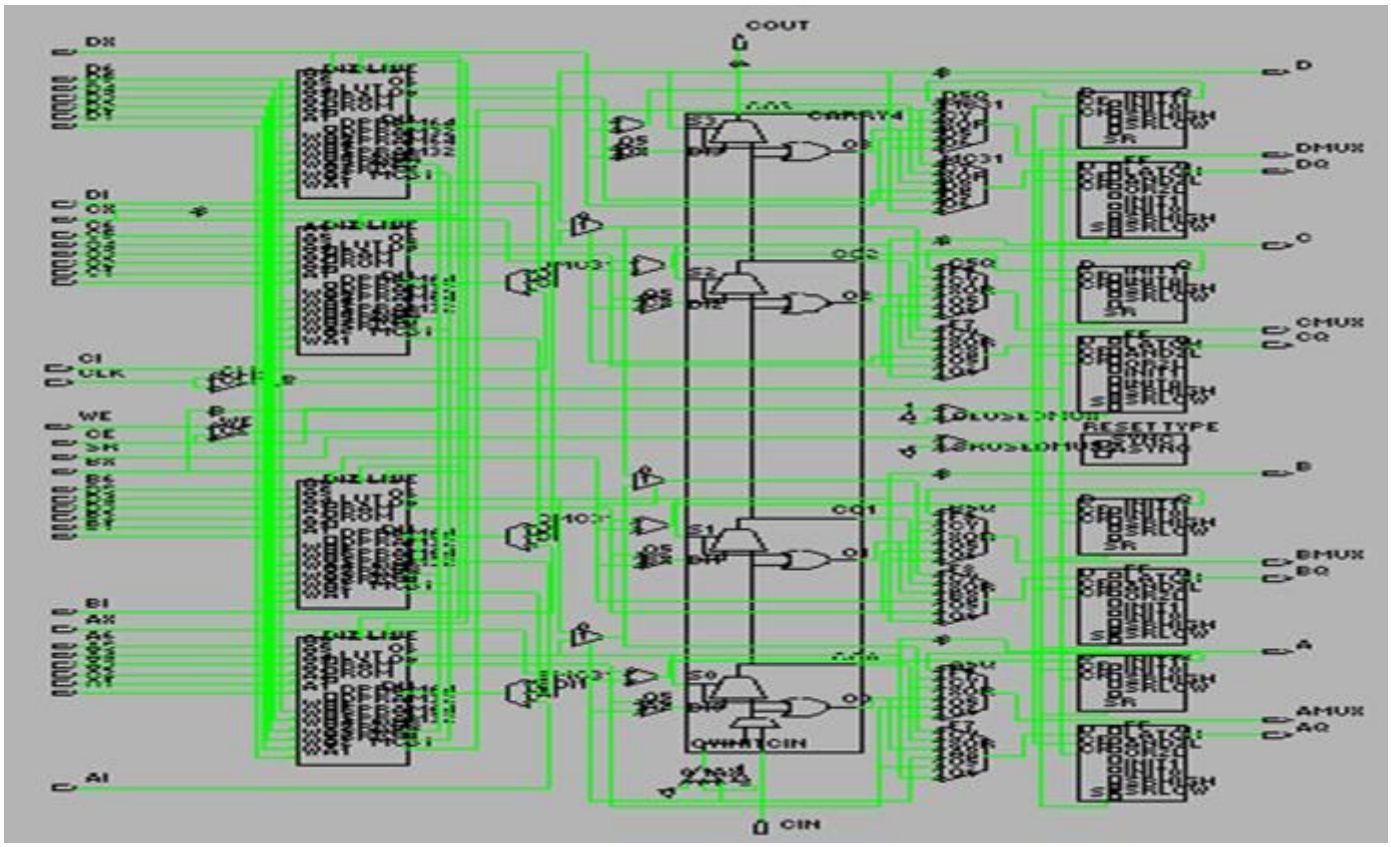

Figure 12

Model of 4x4 OSTBC MIMO using FPGA editor

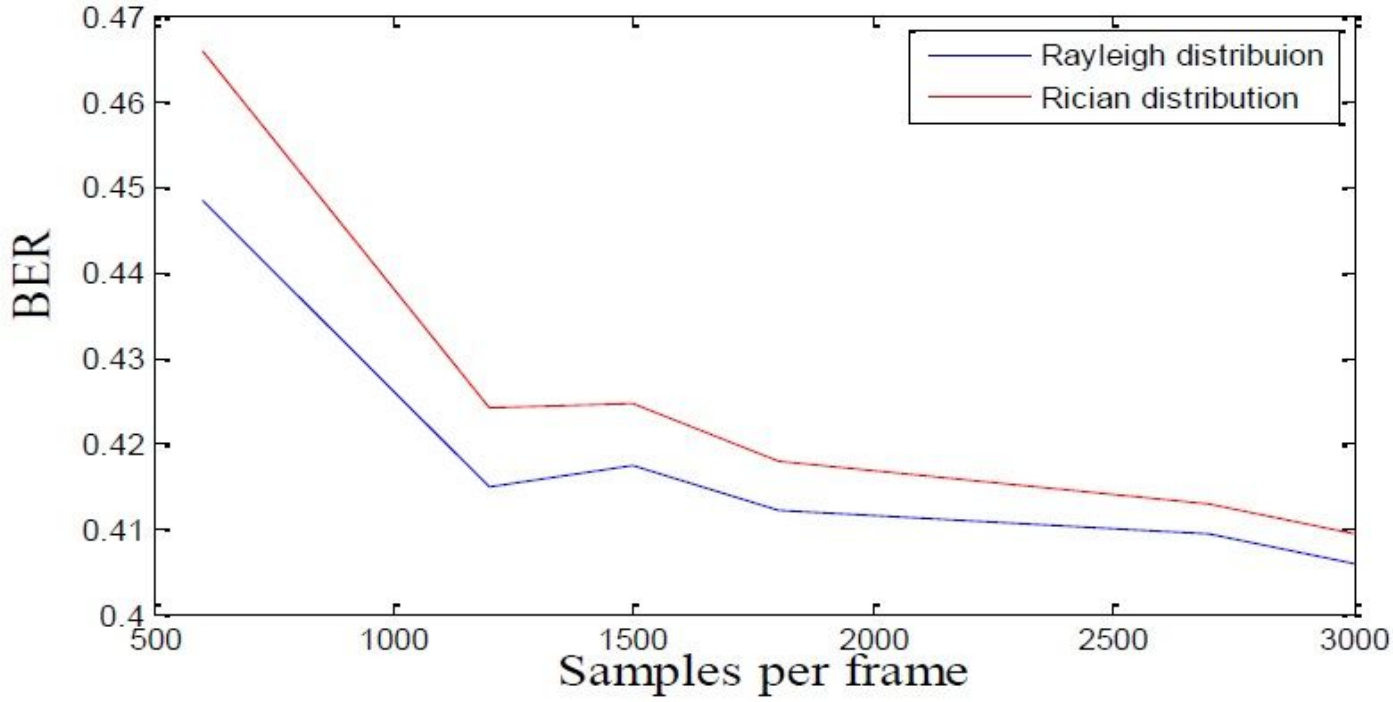

Figure 13

Comparison of BER between Rayleigh fading distribution and Rician fading distribution

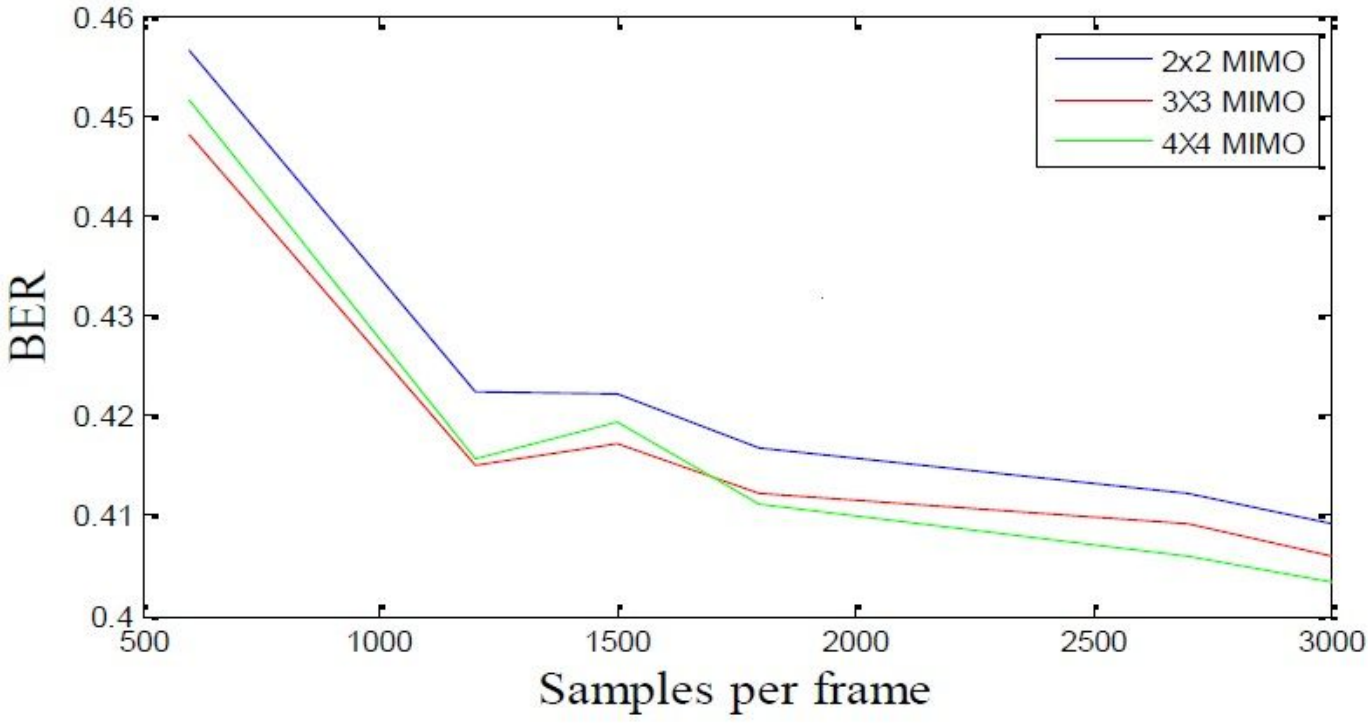

Figure 14

Comparison of BER for different MIMO techniques

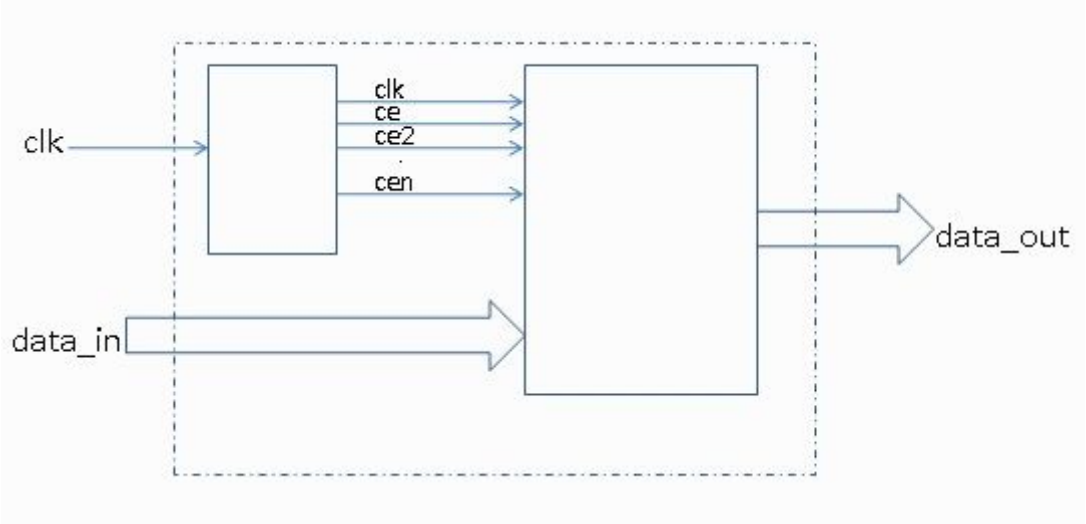

Figure 15

Hardware data sheet for design of Encoder

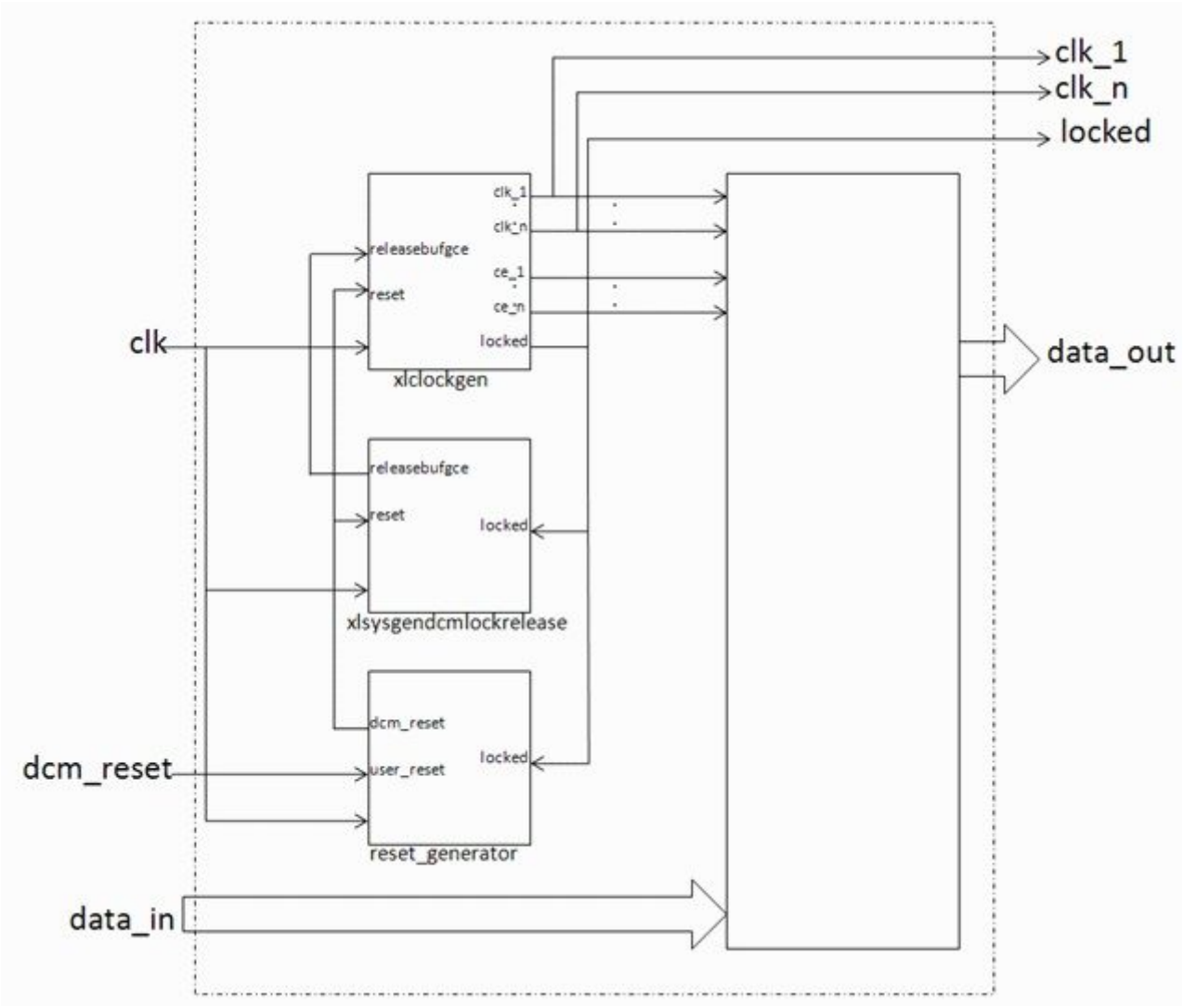

Figure 16

Hardware data sheet for design of Digital clock manager

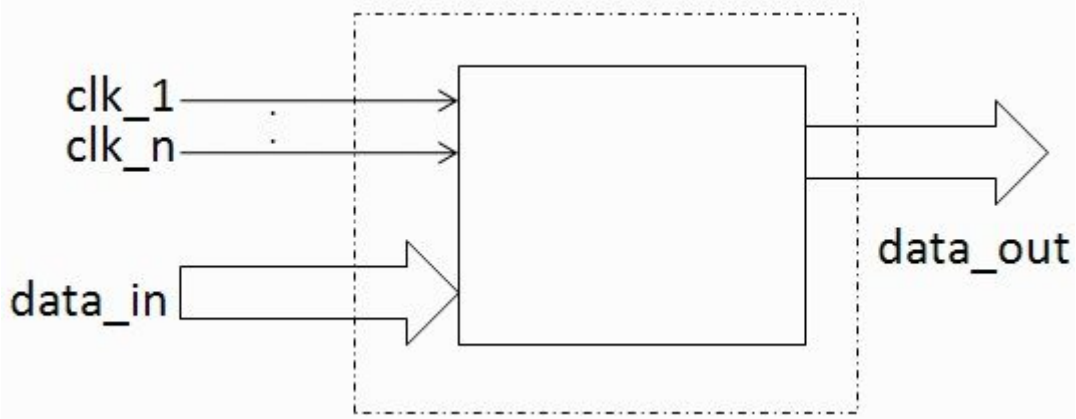

Figure 17

Hardware data sheet for design of multiple clocks

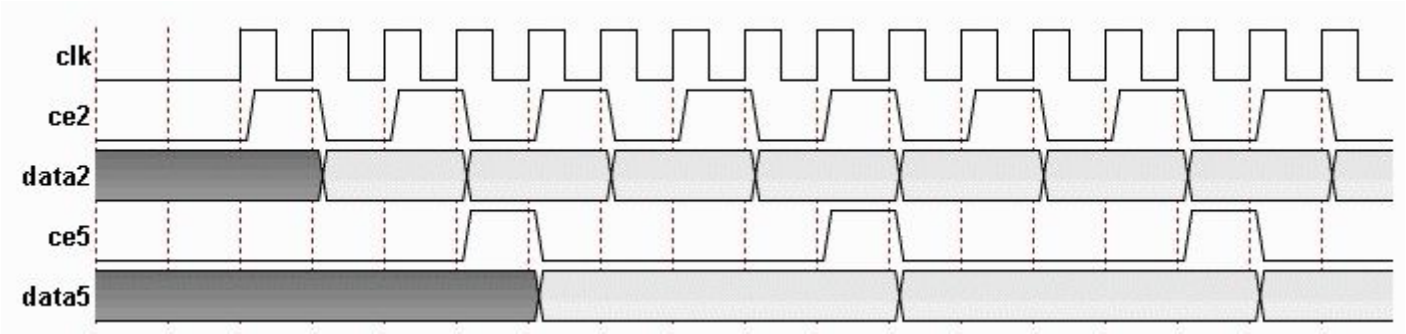

Figure 18

Hardware data sheet of timing diagram

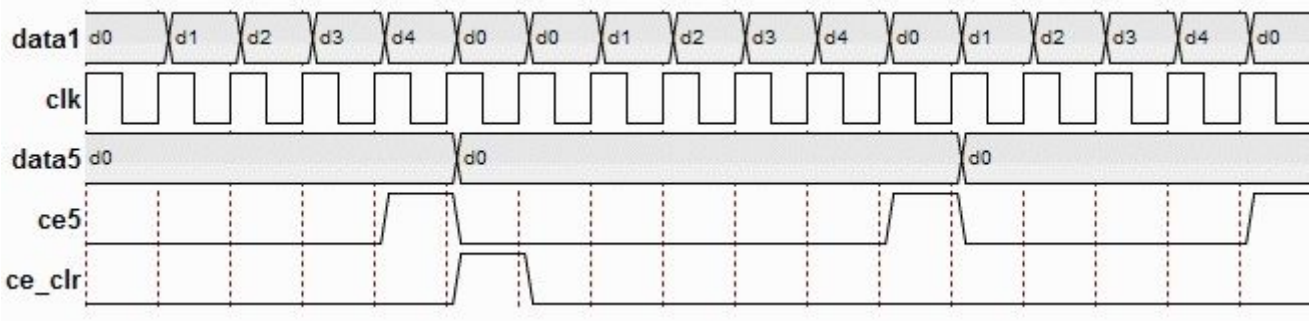

Figure 19

Hardware data sheet of timing diagram for Encoder

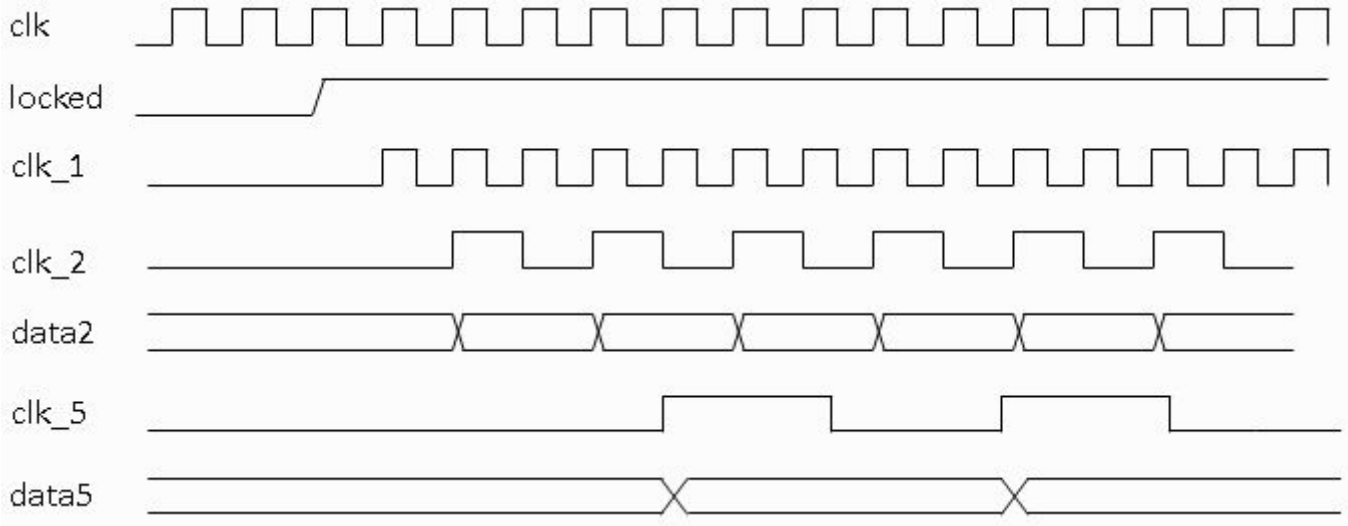

Figure 20

Hardware data sheet of timing diagram for digital clock manager

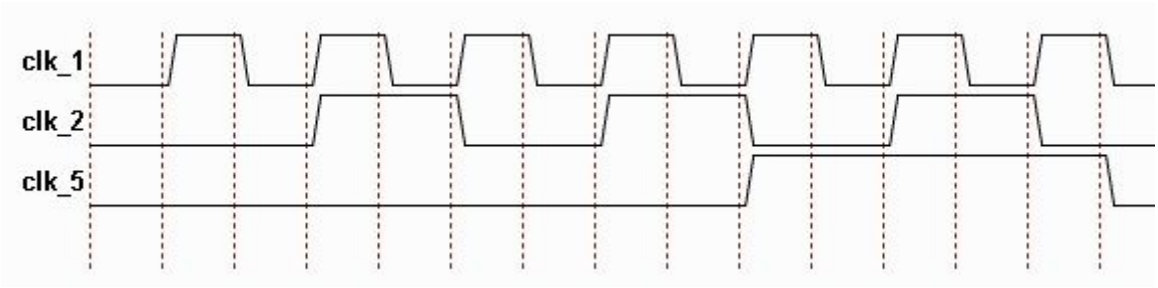

Figure 21

Hardware data sheet of timing diagram for multiple clocks